Recommended acetylene 12 C 2 H 2 line list in 13.6μm spectral region: 2 New measurements and global modeling

D Jacquemart, P Soulard, O Lyulin

Recommended acetylene $^{12}C_2H_2$ line list in 13.6μm spectral region: New measurements and global modeling

D. Jacquemart [a,], P. Soulard [a], O. Lyulin [b]*

[a] Sorbonne Université, CNRS, MONARIS, UMR 8233, 4 place Jussieu, 75005 Paris, France

[b] Laboratory of Theoretical Spectroscopy, V.E. Zuev Institute of Atmospheric Optics, Siberian Branch, Russian Academy of Sciences,1, Academician Zuev Square, 634055 Tomsk, Russia

Number of Figures: 12
Number of Tables: 7
Supplementary materials (electronic files): 5

Please send proofs to: David Jacquemart
Email: david.jacquemart@sorbonne-universite.fr

Keywords : Acetylene; Line positions and intensities; Line list; Spectroscopic databases.

Abstract

Following a previous work on recommended $^{12}C_2H_2$ line list for the 13 − 248 cm^{-1} and 390 − 634 cm^{-1} spectral regions, the present work is dedicated on new measurements between 638 and 820 cm^{-1}. Line intensities have been measured for 18 bands: only four of them were previously reported. The measurements allowed validating predictions based on the global modeling of the line positions and intensities performed within the framework of the method of effective operators. Using the present new measurements as well as previous measurements from literature, new fittings of the line intensities for the $\Delta P = 1$ series of transitions have been performed. A complete calculated line list of 200 bands belonging of the $\Delta P = 1$ series of transitions is proposed as supplementary data in order to improve such spectroscopic databases as HITRAN or GEISA.

1. Introduction

The present work is the continuation of a previous paper [1] concerning calculation between 13 and 248 cm^{-1} and between 390 and 634 cm^{-1} with the aim to produce accurate $^{12}C_2H_2$ calculated line positions and intensities. The line list from Ref. [1] has been recently added in HITRAN2016 database. The calculation is based on the global modeling of the line positions and intensities within the framework of the method of effective operators [2-4] applied to various ΔP series [1,5-9] (P being polyad number defined in Section 3). In the present work new experimental spectra have been recorded and measurements of line intensities have been performed for 1020 transitions belonging to 18 vibrational bands between 638 and 820 cm^{-1}. The positions and intensities of transitions (including those of 14 bands never measured before) are in very good agreement with acetylene line list presented in calculated acetylene database ASD-1000 [10]. This fact insures that the calculated line list in the region of the ΔP=1 series is very close to the measuring data. As consequences, a set of 200 bands has been selected to generate the acetylene calculated line list of 40021 transitions between 389 and 893 cm^{-1}. This line list is available to update atmospheric and planetary databases as HITRAN [11] and GEISA [12]

The experimental spectra recorded in MONARIS laboratory and their analysis will be presented in Section 2. The theoretical approach will be discussed in Section 3. In Section 4, the line intensity new fit for the ΔP = 1 series of bands will be described. Section 5 will be devoted to the description of the recommended $^{12}C_2H_2$ line list and comparisons of calculations with measurements and databases will be presented in Section 6. Note that the reader is addressed to color version of this article for a complete readability of most of the figures.

2. New measurements in the 638 − 820 cm^{-1} spectral region

The previous work [1] was dedicated to $\Delta P = 0$ series, as well as the beginning of $\Delta P = 1$ series with very weak bands recorded with absorption paths of around 150 m. To study weaker bands in the middle of the $\Delta P = 1$ region (13.6 μm), such high absorption path is useless since the spectra will be totally saturated. An absorption path of 25.7 cm has been used to record three high resolution spectra with pressure of acetylene ranging from (2- 10)×10^{-3} atm allowing us to observe 4 bands already studied in literature as well as 14 bands never studied before. Experimental conditions are summarized in Table 1. For that, the Bruker IFS 125 in MONARIS has been equipped with a KBr beam splitter, and a MCT-D316 detector. A Globar source has been used. Temperature in the cell is measured with platinum probes inside the cell (accuracy of ± 0.1K). Pressure of natural acetylene inside the cell is measured with a 10mbar-full scale Baratron gauge (stated accuracy of ± 0.25%). A wavenumber calibration has been performed based on line position of $^{12}C_2H_2$ transitions from HITRAN [11] as etalon. The average correcting factor $\varepsilon = (\sigma_{ref} - \sigma_{obs})/\sigma_{ref}$ has been found equal to -6.6(1)10^{-7} (between parenthesis is 1 standard deviation 1SD). At 700 cm^{-1}, it corresponds to a correction of –0.46(1)×10^{-3} cm^{-1}. The accuracy of absolute line positions measurements is estimated to be equal to 0.1×10^{-3} cm^{-1}.

(Table 1)

Figure 1 shows a portion around 705-706 cm^{-1}, where the strongest saturated line is the $P_{ee}(10)$ transition of the ν_5^1 cold band of $^{12}C_2H_2$. Around 705.243 cm^{-1} the same transition is observed but corresponds to $^{12}C^{13}CH_2$ isotopologue (marked with red stick in the upper panel of Fig. 1). Although only $^{12}C_2H_2$ transitions have been studied in the present work the parameters of such $^{12}C^{13}CH_2$ transitions have been fitted together with nearby lines. HITRAN [11] and GEISA [12] databases contain the 5 most intense vibrational bands in the studying region coming from the Ref. [13,14]. All these bands were reconsidered here except the strongest ν_5^1 band which is saturated in our spectra. Note also that the two bands $(\nu_4+\nu_5)^0_+ - \nu_4^1$ and $(\nu_4+\nu_5)^0_- - \nu_4^1$ present in HITRAN and GEISA from Ref. [13] correspond to only one band noted "00011 1-1 _ 00010 1 0" in the present work using vibrational assignment based on $V_1\ V_2\ V_3\ V_4\ V_5\ \ell_4\ \ell_5$ quantum numbers (see Section 3.2 of Ref. [1] for more details).

The peak to peak signal-to-noise ratio of the spectra is almost constant with the wavenumber and is around 70. As it can be guessed in Fig. 1, a multiplicative channel spectrum is observed on all experimental spectra. This channel spectrum was modelled locally

as a background adjusted by a second order polynomial function within spectral domains around 0.04-0.1 cm^{-1}.

(Figure 1)

The multispectrum fitting procedure of Ref. [15] was used fixing the self-broadening coefficients at the values of Ref. [16] and using the Voigt profile. The apparatus function has been calculated with the maximum of optical path difference equal to 225 cm and the nominal value of the radius of the beam inside the interferometer equal to 1.0 mm together with the focal distance equal to 418 mm. An example of the result of the multispectrum fit is given in Fig. 2 for the P_{ee} (24) transition of the $2\nu_5^2$ band of $^{12}C_2H_2$ between 675.809 and 675.849 cm^{-1}. Taking into account the signal to-noise ratio (which is close to 70), the residuals of the fit do not show any strong characteristic signature despite a kind of asymmetry in the profile that gives residuals slightly larger than the 1.5 % peak to peak noise of the experimental spectra.

(Figure 2)

Absolute line intensities have been retrieved for 1220 transitions involving 18 vibrational bands. The accuracy of line intensities has been estimated to be around 5% for transitions deep enough in recorded experimental spectra (with intensities around 10^{-20}–10^{-21} cm^{-1}/(molecule.cm^{-2})) whereas the accuracy may reach up to 10% for weaker transitions (with intensities around 10^{-22}–10^{-23} cm^{-1}/(molecule.cm^{-2})). A sample of the results for the $2\nu_5^0 - \nu_5^1$ band is given in Table 2 (the whole set of the measurements is given in Supplementary material 1). A summary of the measurements performed in this work is presented in Table 3 for the 18 studied bands.

(Table 2)

(Table 3)

3. Theoretical approach

Measured line intensities were included in the simultaneous fit of the effective dipole moment parameters using approach describing in many previous publications (see for example [1-5]). The most important points of the approach are given below. The probability of a transition between two states $W_{b\leftarrow a}$ can be deduced from every line intensity expressed in cm^{-1}/(molecule∗cm^{-2}) using following conventional formula:

$$S_{b\leftarrow a}(T) = \frac{8\pi^3 g_i \sigma_{b\leftarrow a}}{3hcZ_{tot}(T)} e^{-\frac{hcE_a}{k_B T}} \left(1 - e^{-\frac{hc\,\sigma_{b\leftarrow a}}{k_B T}}\right) W_{b\leftarrow a}\,, \quad (1)$$

where h is the Planck's constant equal to 6.6260755×10^{-27}erg.s (1 erg =10^{-7} J); c is the vacuum velocity of light equal to 2.99792458 10^{10} cm s^{-1}; $\sigma_{b\leftarrow a}$ is the transition wavenumber in cm^{-1}; E_a is the energy of the lower state (ground state) in cm^{-1}, k_B is the Boltzmann's constant equal to 1.380658 × 10^{-16}erg.K^{-1}; g_i is the statistical weight due to nuclear spin of the lower levels (equal 3/1 for symmetry *a*/*s*), and T is the temperature of the measurements which was 296 K in our case. The total partition function Z_{tot} used in this work is equal to 412.45 at 296 K [17]. The probability of a transition $W_{b\leftarrow a}$ is related to the dipole moment matrix element by the next expression (m is the projection of the angular moment on the Z axis of the space fixed system of axes):

$$W_{b\leftarrow a} = 3\sum_{mm'} |\langle \Psi_b | M_Z | \Psi_a \rangle|^2. \quad (2)$$

In Ref. [4] the eigenfunctions of the effective Hamiltonian of acetylene molecule have been obtained in the form of expansion over products of harmonic oscillator and rigid rotator wavefunctions:

$$\Psi_{NJMm_\varepsilon}^{eff} = \sum_{V_1V_2V_3V_4V_5\ell_4\ell_5} C_{NJ\varepsilon}^{V_1V_2V_3V_4V_5\ell_4\ell_5} |V_1V_2V_3V_4V_5\ell_4\ell_5 JmK\varepsilon\rangle, \quad (3)$$

where N identify the eigenstate inside of the polyad of interacting vibrational levels, V_i are the harmonic oscillator quantum numbers, ℓ_i are the vibrational angular moments of the degenerate oscillators, J –angular moment quantum number, K is the projection of the angular moment on

the axis of the molecule, ε is the Wang combination symmetry (*e*/*f*) and *C* are the mixing coefficients. The sum is performed over all interacting basic functions forming one polyad which is defined by polyad number *P*. In the case of acetylene molecule, the harmonic oscillator quantum numbers of the interacting basic functions should satisfy the equation:

$$P = 5V_1 + 3V_2 + 5V_3 + V_4 + V_5 = const, \tag{4}$$

which expresses the approximate relations between normal mode frequencies in this molecule.

In order to use these functions in our calculation the dipole moment operator was transformed to the effective dipole moment operator using the same unitary transformation as the one transforming vibrational-rotational Hamiltonian to the effective:

$$W_{N'J'\varepsilon'\leftarrow NJ\varepsilon} = 3\sum_{mm'}\left|\left\langle \Psi_{NJm'\varepsilon'}^{eff} \middle| M_Z^{eff} \middle| \Psi_{NJm\varepsilon}^{eff}\right\rangle\right|^2 =$$

$$= 3\sum_{mm'}\left|\sum_{\mathbf{V}\boldsymbol{\ell},\mathbf{V}'\boldsymbol{\ell}'} C_{NJ\varepsilon}^{\mathbf{V}\boldsymbol{\ell}} C_{N'J'\varepsilon'}^{\mathbf{V}'\boldsymbol{\ell}'} \left\langle V'\boldsymbol{\ell}'J'K'm'\varepsilon' \middle| M_Z^{eff} \middle| V\boldsymbol{\ell}JKm\varepsilon\right\rangle\right|^2, \tag{6}$$

where we denoted for simplicity the set of the harmonic oscillator quantum numbers V_i by vector **V** and the vibrational angular moment quantum numbers ℓ_i by vector $\boldsymbol{\ell}$. The sum over these vectors assumes the sum over every quantum numbers separately, but satisfying Eq. (4). After developing effective dipole moment operator in series the calculations lead to the next expression for the probability of the transition:

$$W_{N'J'\varepsilon'\leftarrow NJ\varepsilon} = (2J+1)\left|\sum_{\mathbf{V}\boldsymbol{\ell},\mathbf{V}'\boldsymbol{\ell}'} C_{NJ\varepsilon}^{\mathbf{V}\boldsymbol{\ell}} C_{N'J'\varepsilon'}^{\mathbf{V}'\boldsymbol{\ell}'} \sqrt{f_{\Delta\mathbf{V}}^{\Delta\boldsymbol{\ell}}(\mathrm{V},\boldsymbol{\ell})\left(1+\left|\delta_{\ell_4,0}\delta_{\ell_5,0}-\delta_{\ell_4',0}\delta_{\ell_5',0}\right|\right)}\times\right.$$

$$\left.\times\Phi_{\Delta J\Delta K}(J,K) M_{\Delta\mathbf{V}}^{\Delta\boldsymbol{\ell}}\left(1+\sum\nolimits_i K^{\Delta\mathbf{V}_i\Delta\boldsymbol{\ell}} V_i + \sum\nolimits_{i=4,5} a^{\Delta\mathbf{V}_i\Delta\boldsymbol{\ell}}(2\ell_i\Delta\ell_i+1) + F_{\Delta J\Delta K}^{\Delta\mathbf{V}\Delta\boldsymbol{\ell}}(J,K)\right)\right|^2. \tag{7}$$

The square of the function $\Phi_{\Delta J\Delta K}(J,K)$ multiplied by factor (2*J*+1) gives the Hönl-London factor in the case of isolated transitions. For ΔK=0,±1 this function coincide with Clebsch-Gordan coefficients and for ΔK=±2, ±3 can be found in Ref. [5,18]. The function $f_{\Delta\mathbf{V}}^{\Delta\boldsymbol{\ell}}(\mathrm{V},\boldsymbol{\ell})$ is the square of vibrational matrix element and can be found in Ref. [5]. The combination of the Kronecker symbols appears due Wang basis functions and provides 2 when one of the basic functions has both vibrational angular moments equal zero. The Herman-Wallis type factor $F_{\Delta J\Delta K}^{\Delta\mathbf{V}\Delta\boldsymbol{\ell}}(J,K)$ describes the rotational dependence of the effective dipole moment operator. For ΔK=±1 it can be written as follows:

for Q branch:

$$F^{\Delta\mathbf{V}\Delta\boldsymbol{\ell}}_{\Delta J\Delta K}(J,K) = -\frac{1}{2}b^{\Delta\mathbf{V}}_{f}{}^{\Delta\boldsymbol{\ell}}(2K\Delta K+1) + d^{\Delta\mathbf{V}}_{fQ}{}^{\Delta\boldsymbol{\ell}}\Big[J(J+1) - K^2 - \Delta K(K+\tfrac{\Delta K}{2})\Big], \qquad (8)$$

for P and R branches:

$$F^{\Delta\mathbf{V}\Delta\boldsymbol{\ell}}_{\Delta J\Delta K}(J,K) = -\frac{1}{4}\big(d^{\Delta\mathbf{V}}_{fQ}{}^{\Delta\boldsymbol{\ell}} - d^{\Delta\mathbf{V}}_{f}{}^{\Delta\boldsymbol{\ell}}\big) - \frac{1}{2}\big(b^{\Delta\mathbf{V}}_{f}{}^{\Delta\boldsymbol{\ell}} + d^{\Delta\mathbf{V}}_{fQ}{}^{\Delta\boldsymbol{\ell}}\big)(2K\Delta K+1) - d^{\Delta\mathbf{V}}_{fQ}{}^{\Delta\boldsymbol{\ell}}K^2 +$$

$$+ b^{\Delta\mathbf{V}}_{f}{}^{\Delta\boldsymbol{\ell}}m + d^{\Delta\mathbf{V}}_{f}{}^{\Delta\boldsymbol{\ell}}m^2 + \frac{1}{2}\big(d^{\Delta\mathbf{V}}_{fQ}{}^{\Delta\boldsymbol{\ell}} - d^{\Delta\mathbf{V}}_{f}{}^{\Delta\boldsymbol{\ell}}\big)m(2K\Delta K+1). \qquad (9)$$

In the case ΔK=0 for P and R branches, the Herman-Wallis type factor $F^{\Delta\mathbf{V}\Delta\boldsymbol{\ell}}_{\Delta J\Delta K}(J,K)$ is:

$$F_{\Delta f\,\Delta K=0}{}^{\Delta\mathbf{V}\Delta\boldsymbol{\ell}}(J,K) = b^{\Delta\mathbf{V}}_{f}{}^{\Delta\boldsymbol{\ell}}m + d^{\Delta\mathbf{V}}_{f}{}^{\Delta\boldsymbol{\ell}}\big[J(J+1) - K^2 + m\big]. \qquad (10)$$

The m quantity in the Eqs. (9-10) and corresponds to m = –J, J+1 for P, R branches respectively, and should not be confounded with the angular moment projection quantum number used in Eqs. (2,3,6). The expression $F^{\Delta\mathbf{V}\Delta\boldsymbol{\ell}}_{\Delta J\Delta K}(J,K)$ for the Q branch (ΔK=0) depends from $\boldsymbol{\ell}_4$ and $\boldsymbol{\ell}_5$ values and can be found in Ref. [3]. The set of the effective dipole moment parameters: $M^{\Delta\boldsymbol{\ell}}_{\Delta\mathbf{V}}$, $K^{\Delta\mathbf{V}}_{i}{}^{\Delta\boldsymbol{\ell}}$, $a^{\Delta\mathbf{V}}_{i}{}^{\Delta\boldsymbol{\ell}}$, $b^{\Delta\mathbf{V}}_{f}{}^{\Delta\boldsymbol{\ell}}$, $d^{\Delta\mathbf{V}}_{f}{}^{\Delta\boldsymbol{\ell}}$, $d^{\Delta\mathbf{V}}_{fQ}{}^{\Delta\boldsymbol{\ell}}$ determines the intensity distribution in the spectral domain defined by the value of ΔP. Note, that the effective dipole moment parameters are the same for the vectors $\Delta\mathbf{V}$ and $\Delta\boldsymbol{\ell}$ differing only by signs except parameter $a^{\Delta\mathbf{V}}_{i}{}^{\Delta\boldsymbol{\ell}}$ which changes the sign when the sign of the vector $\Delta\boldsymbol{\ell}$ changes.

4. Line intensity fit ($\Delta P = 1$ series of transitions)

Based on the new measurements performed in this work (Section 2) and on the measurements published earlier [1,13,14], 14 effective dipole moment parameters have been fitted for the ΔP=1 series of transitions to 1923 measured line intensities belonging to 28 different bands-(see Table 5). Most of the bands measured in this work (13 from 18) correspond to $\Delta V_5 = 1$, with $\Delta \ell_4 = 0$ and $\Delta \ell_5 = 1$, but also with $\Delta \ell_4 = -2$ and $\Delta \ell_5 = +1$ (3 bands), or with $\Delta \ell_4 = -2$ and $\Delta \ell_5 = +3$ (1 band), or with $\Delta \ell_4 = +2$ and $\Delta \ell_5 = +1$ (1 band). No any new effective dipole moment parameter was required to reproduce the new measurements. The set of the fitted effective dipole moment parameters for $\Delta P = 1$ is presented in Table 4 and the statistics of the fit is given in Table 5. For some transitions (weakest or blended), measurements of this work or from Ref. [1,13,14] become less accurate and can be off by more than 10 % from calculations. Most of these measurements have been excluded from the fit of the parameters of Table 4 (representing 424 measurements from a total number of measurements equal to 2347). The present global model (using newly fitted parameters, see Table 4) reproduced 76% (1455 measurements) of the measurements included in the effective dipole moment parameters fit within ± 5%, and 22% of measurements (430 measurements) within ± 5-10%. The eigenfunctions of our global effective Hamiltonian [4] were used in the fit. The weighted dimensionless standard deviation χ = 0.75 and the root mean squares of the residuals RMS=4.4% were obtained in result of fit. The effective dipole moment parameters retrieved in this work are consistent with previous ones except for the b_J parameter for $\Delta V_4 = 0$, $\Delta V_5 = 1$, $\Delta \ell_4 = 0$, and $\Delta \ell_5 = 1$ that converges to $-0.49(3) \times 10^{-3}$ in the present fit instead of $-0.76(5) \times 10^{-3}$ and $-0.72(5) \times 10^{-3}$ in Ref. [1] and Ref. [4] respectively (see Table 4). For bands measured in the present work, the 3 sets of effective dipole moment parameters in Table 4 lead to similar calculations able to reproduce the intensities of transitions never measured before.

(Table 4)

(Table 5)

Examples of calculations and measurements for two newly measured bands are given in Figs. 3-4. Similar graphic comparisons are available for all measured bands in Supplementary material 2. As observed in Figs. 3-4, the differences between different calculations are negligible. Both calculations from effective parameters of Refs. [1,4] and of this work (see Table 4) are similar and reproduce the rotational dependence of R^2 for the 14 bands newly observed in this work. As observed in Figs. 3-4, the rotational dependence of measured R^2 values is quite smooth and well reproduced by all calculations (all calculations may not always

be distinguished because of the scale and of the similar calculated values). For some branches, one can clearly see that the measured rotational dependence of $R^2(m)$ cannot be reproduced by Herman-Wallis factors.

(Figure 3)

(Figure 4)

5. Recommended acetylene ($^{12}C_2H_2$) line list for databases

Using the effective Hamiltonian parameters of Ref. [4] and effective dipole moment parameters (see Table 4) of $\Delta P = 1$ series, the acetylene ($^{12}C_2H_2$) line list has been generated in the studding region with intensity cut off 10^{-28} cm^{-1}/(molecule.cm^{-2}). The spectral lines in this model do not have a unique vibrational labeling for all transitions belonging to a same band, but two principal contributors are given for upper and lower levels of transitions which can change inside a band. In order to have consistent vibrational labelling for a same series of transitions (with *P*, *Q* and *R* branches), an algorithm has been developed to reveal levels crossings. Indeed, as pointed out in Ref. [1], for some bands the main contributor to the eigenfunctions can change within a same series of transitions (band). When ro-vibrational levels of different series of transitions, considering as *J* function, approach, some levels crossing can appear. As performed in Ref. [1], the vibrational assignment of the lowest *J* transitions has been used to name the band. Inside a series of transitions, when crossings appear, the algorithm is looking for the next transition belonging to the series using such criteria as the difference of wavenumbers between transitions and the two largest contributions of the basic functions (for the upper and lower levels). Such transitions are noted with a star in the Table 6 and Supplementary material 3. The fact that the main contributor to the eigenfunctions is changing progressively (slowly or quickly depending on bands) affect line intensities in an unusual way so that Herman-Wallis factors are unable to reproduce the rotational dependence of transition dipole moment squared R^2. This problematic has been pointed out for example in Ref. [19] for $\nu_1+\nu_3+2\nu_4^0$ band (see Fig. 3 of Ref. [19]) and in Ref. [1] for 2 bands (see Figs. 10-11 of Ref. [1]) where the Herman-Wallis factors were not adapted to fit such unusual rotational dependence. Interesting case of band crossing is also presented in Ref. [20]. In the present work, several newly observed bands demonstrate such smooth rotational dependence of R^2 and are well predicted by previous calculations [1,4]. The effects of crossing levels can be drastic for line intensities calculation. The case of the 00031 1 1 – 00030 1 0 band is discussed as an example. The line intensities and transition dipole moment squared

values in the Q_{fe} branch are plotted in Figs. 5 and 6 respectively. Extract of the whole calculation (available as Supplementary material 4) with the two main contributors to the vibrational levels is given in Table 6 for the Q_{fe} branch of the 00031 1 1 – 00030 1 0 band. The first crossing appears in the Q_{fe} branch at J equal 17, the first contributor in the upper state becomes 00031 1-1 instead of 00031 1 1. Then at J equal 18, the first contributor in the upper state changes again to become 00031 3 1 for the rest of the branch. Such crossings led to a change of slope for the R^2 values inside the branch (see Fig. 6). As written before, such rotational dependence within a branch cannot be correctly fitted by Herman-Wallis factors. In Fig. 5 one can observe the line intensities getting stronger after the crossing point (J =18, see Fig. 5). One can also notice in Fig. 5 the alternation of intensities versus J with a ratio 3:1 for $^{12}C_2H_2$ (due to the nuclear spins for symmetric isotopologues).

(Figure 5)

(Figure 6)

(Table 6)

From the complete calculation, 200 series of transitions forming vibrational bands have been defined and selected for databases. The whole line list contains 41021 transitions. Two cut-off procedures have been applied to select transitions. First a line intensity cut-off equal to 10^{-28} cm^{-1}/(molecule.cm^{-2}) at 296K has been used. Then, only bands with a sum of line intensities greater than 10^{-24} cm^{-1}/(molecule.cm^{-2}) at 296K have been selected. Note that the sum of line intensities has been halved when the band is affected by ℓ–type doubling (leading to two series of P, Q and R branches). A summary of the present calculation for the 30 strongest bands is given in Table 7. The whole summary for the 200 bands calculated in the recommended line list is given as Supplementary material 4. Note, the recommended line list includes also most of bands proposed in Ref. [1] and already in HITRAN2016. These bands are marked by "H" letter in the Table 7 and corresponding Supplementary material 4. Because of the line intensity cut-off procedures performed in the present work, the 7 weakest bands from Ref. [1] are not included in the present line list.

(Table 7)

For all 200 bands a line list in HITRAN format has been generated and is available in Supplementary material 5 to this paper. As discussed in Section 6, the line positions from Refs. [21,22] present in HITRAN2016 have been used (when available) for the 5 strongest bands using same error code than in HITRAN2016: 4 (between 0.1×10^{-3} and 1×10^{-3} cm^{-1}). For other

transitions, the calculated line positions of the present work (coming from effective Hamiltonian parameters of Ref. [4]) have been used with an error code equal to 3 (corresponding to $(1 - 10)\times10^{-3}$ cm^{-1}) for transitions with J lower or equal to 40 and with an error code equal to 2 (corresponding to $(10 - 100)\times10^{-3}$ cm^{-1}) for transitions with J higher than 40 (see discussion in Section 6). The set of effective dipole moment parameters from the present work (see Table 4) has been used to generate line intensities of all bands except the cold ν_5^1 band for which the set of effective dipole moment parameters from Ref. [1] has been used in order to be more consistent with measurements (see discussion in Section 6). For line intensities a code 5 (between 5 and 10%) was used for the 18 measured bands (noted "Obs" in Table 7), whereas for a predicted band the error code 4 (≥10% and <20%) was chosen allowing to distinguish easily predicted and measured bands. Broadening coefficients (self and air), temperature dependence of air-broadening coefficients, air-shifting coefficients and associated error codes have been added following recommendations of Ref. [23] included in HITRAN2004 edition [24]. However, the error codes of air- and self-broadening coefficients have been degraded from 6 (between 2 and 5%) to 4 (between 10-20%) when $J \geq 35$ since a constant estimated value is used. Let us mention that in HITRAN 2016, error codes for broadening coefficients are all fixed to 6 even for transitions with J greater than 35.

Note that the vibrational labeling used in the present work has been described in Section 3.2 of Ref. [1]. We urge spectroscopic databases to note the fact that using V_1 V_2 V_3 V_4 V_5 ℓ_{tot} quantum numbers instead of V_1 V_2 V_3 V_4 V_5 ℓ_4 ℓ_5 quantum numbers will lead to various transitions with identical assignments. The FORTRAN format A15 for vibrational assignment should change to (1X,3I1,4I2,A1,I1,A1) respectively for V_1, V_2, V_3, V_4, V_5, ℓ_4, ℓ_5, quantum numbers, the u/g symmetry, a ranking number (noted r in HITRAN, see Table 3 of Ref. [24]), and the +/- symmetry. V_4 and V_5 being the lowest energy vibrational modes, two digits should be reserved for these modes for the possibility to have V values greater than 9. The ranking number is not used in the present line list and should not be useful anymore.

A sample of synthetic spectra using either HITRAN2016 or the present recommended line list are compared to experimental spectrum 3 in Fig. 7 between 703 and 706 cm^{-1}. One can notice the many transitions of $^{12}C_2H_2$ missing in HITRAN2016 [11] and GEISA2015 [12] but present in our line list. One can also observe some missing absorption features due to $^{12}C^{13}CH_2$ isotopologue noted by symbols in Fig. 7 and assigned in Ref. [25].

(Figure 7)

6. Comparisons with spectroscopic databases

Since our aim is to update line positions and intensities already present in atmospheric databases and upgrade the line list with many hot bands, comparisons have been performed with HITRAN2016 edition. HITRAN2016 [11] or GEISA2015 [12] have same data for $^{12}C_2H_2$ line positions and intensities of strong bands from Refs. [13,14], except for weak bands from Ref. [1] included in HITRAN2016 edition [11]. Calculations performed in Ref. [1] for the 29 bands in $\Delta P = 1$ spectral region, and in the present work are based on same formalism [4] so no comparison is performed. Note that none of the bands measured in the present work is in common with the bands studied in Ref. [1]. Comparisons with EXOMOL database for $^{12}C_2H_2$ [26] are also performed in term of line positions and intensities.

In the $\Delta P = 1$ absorption region, line intensities of the 5 strongest bands at room temperature present in HITRAN are coming from Refs. [13,14]. Herman-Wallis factors and vibrational transition dipole moments squared from Refs. [13,14] have been used to generate calculated line intensities for updating HITRAN2004 edition [24]. Extrapolations for high *J*-values in HITRAN were performed using fixed R^2 values equal to the calculated one for the last measured transition in the branch. The present global calculation is consistent with HITRAN line intensities and improves extrapolations performed in HITRAN with fixed transition dipole moment squared values. Examples for the ν_5^1 and $2\nu_5^0 - \nu_5^1$ bands are given in Figs. 8-9 respectively. Figure 9 shows the very good consistency of present measurements and those from Ref. [13]. No measurement has been performed in this work for the strong ν_5^1 band, but calculations and measurements from literature plotted in Fig. 8 shows a slight discrepancy (up to 4% for highest *J* values) between measurements and calculations in the *R*-branch, especially with parameters of the present work (see Table 4). The R^2 values deduced from EXOMOL line intensities are also given in Figs. 8 and 9. One can notice that EXOMOL line intensities worse reproduce measurements showing inaccurate rotational dependences especially for *P* and *R* branches. The whole set of graphic comparisons is available in Supplementary material 2.

(Figure 8)

(Figure 9)

Line positions of the 5 strongest bands from HITRAN2016 coming from calculation of Refs. [21,22] (believed to be a reference in the $\Delta P = 1$ region for line positions) were compared with ASD-1000 calculated line positions [10] and with present measurements. Comparisons plotted in Fig. 10 versus line intensity show that for the weakest transitions the differences between HITRAN and ASD-1000 calculation can reach ±0.03 cm^{-1} while present measurements and HITRAN2016 positions are in very good agreement. In order to better

understand the situation, the differences have been plotted versus *m* for the 00001 0 1 – 00000 0 0 and 00011 1 1 – 00010 1 0 bands in Fig. 11 and 12 respectively, including also comparisons with EXOMOL line positions [26]. One can clearly observe in these figures increasing of deviations of ASD-1000 and EXOMOL line positions from HITRAN values for large rotational quantum numbers *J*. Moreover, while for the 00001 0 1 – 00000 0 0 band (Fig.11) the differences increase on average in the same way for ASD-1000 and EXOMOL, for the 00011 1 1 – 00010 1 0 band the trend is opposite (Fig.12). In term of line positions, the global model [4] does not allow to reach the accuracy of more simple models as those from Refs. [21,22] (used in HITRAN for the 5 strongest bands). These models consider several resonance interactions between ro-vibrational states and can well describe the rotational dependence of the energy of several interacting states. The models used in Refs. [21,22] allowed to reach estimated accuracy equal to ±0.0001 cm^{-1} [21]. As consequences the line positions in HITRAN have been kept in our recommended line list for the 5 strongest bands as discussed in Section 5.

(Figure 10)

(Figure 11)

(Figure 12)

6. Conclusion

Recent measurements from Ref. [1] and from the present work allowed to demonstrate the predictive capabilities of global calculation [4] for $\Delta P = 1$ series of bands. This calculation has been used to generate a complete line list in HITRAN format for $^{12}C_2H_2$ isotopologue between 389 and 893 cm^{-1}. The cut-off procedures used to select the most intense bands will allow to model acetylene absorption features with better accuracy for atmospheric temperature spectra, but also to model higher temperature spectra since the recommended line list contains many hot bands. The present recommended line list can be considered as a revised selection of bands from the high-temperature acetylene spectroscopic databank (ASD-1000) [10] in the $\Delta P = 1$ spectral region, adapted for spectroscopic databases such as HITRAN or GEISA. By performing measurements in higher ΔP spectral regions for weaker bands never measured, the validation of the predictive capabilities of global calculation for higher ΔP absorption regions is planned to improve higher spectral regions in spectroscopic databases.

Acknowledgment

We are grateful to Valery Perevalov from Tomsk V.E. Zuev Institute of Atmospheric Optics for initiating this work and fruitful discussions of the results. We thank Jonathan Tennyson and Sergei Yurchenko for acetylene line list extraction at 296K from EXOMOL. This work was supported by the Ministry of Science and Higher Education of the Russian Federation and by CNRS (France) in the frame of International Research Project SAMIA

References:

[1] Jacquemart D, Lyulin O, Perevalov VI. Recommended acetylene line list in the 20-240cm^{-1} and 400-630 cm^{-1} regions: New measurements and global modeling. J Quant Spectrosc Radiat Transfer 2017;203:440–53.

[2] Perevalov VI, Lobodenko EI, Teffo JL. Reduced effective Hamiltonian for global fitting of C_2H_2 rovibrational lines, in: 12th Symposium and School on High Resolution Molecular Spectroscopy, Proc. SPIE 3090, 1997, pp. 143–149.

[3] Perevalov VI, Lyulin OM, Teffo JL. Global description of the vibrational-rotational line intensities of the acetylene molecule. The approach and calculation formula. Atmos Oceanic Opt 2001;14:730–8.

[4] Lyulin OM, Perevalov VI. Global modelling of vibration-rotation spectra of the acetylene molecule. J Quant Spectrosc Radiat Transfer 2016;177:59–74.

[5] Perevalov VI, Lyulin OM, Jacquemart D, Claveau C, Teffo JL, Dana V, Mandin JY, Valentin A. Global fitting of line intensities of acetylene molecule in the infrared using the effective operator approach. J Mol Spectrosc 2003;218:180-9.

[6] Lyulin OM, Perevalov VI, Mandin JY, Dana V, Jacquemart D, Régalia-Jarlot L, Barbe A. Line intensities of acetylene in the 3-μm region: New measurements of weak hot bands and global fitting. J Quant Spectrosc Radiat Transfer 2006;97:81–98.

[7] Lyulin OM, Perevalov VI, Mandin JY, Dana V, Gueye F, Thomas X, Von der Heyden P, Décatoire D, Régalia-Jarlot L, Jacquemart D, Lacome N. Line intensities of acetylene: Measurements in the 2.5-μm spectral region and global modeling in the Δp=4 and 6 series. J Quant Spectrosc Radiat Transfer 2007;103:496–523.

[8] Lyulin OM, Perevalov VI, Tran H, Mandin JY, Dana V, Régalia-Jarlot L, Thomas X, Décatoire D. Line intensities of acetylene: New measurements in the 1.5-μm spectral region and global modelling in the ΔP=10 series. J Quant Spectrosc Radiat Transfer 2009;110:1815–1824.

[9] Lyulin OM, Perevalov VI. Effective dipole moment parameters of $^{12}C_2H_2$ for the 100, 7.7, 1.4, 1.3, 1.2 and 1.0 μm regions. J Mol Spectrosc 2011;266:75–80.

[10] Lyulin OM, Perevalov VI. ASD-1000: High-resolution, high-temperature acetylene spectroscopic databank. J Quant Spectrosc Radiat Transfer 2017;201:94–103.

[11] Gordon IE, Rothman LS, Hill C, Kochanov RV et al. The HITRAN2016 molecular spectroscopic database. J Quant Spectrosc Radiat Transfer 2017;000:1–66.

[12] Jacquinet-Husson N, Armante R, Scott NA, Chédin A, et al. The 2015 edition of the GEISA spectroscopic database. J Mol Spectrosc 2016;327:31–72

[13] Jacquemart D, Claveau C, Mandin JY, Dana V. Line intensities of hot bands in the 13.6 μm spectral region of acetylene $^{12}C_2H_2$. Journal of Quantitative Spectroscopy and Radiative Transfer 2001; 69:81–101.

[14] Mandin JY, Dana V, Claveau C. Line intensities in the ν_5 band of acetylene $^{12}C_2H_2$. J Quant Spectrosc Radiat Transfer 2000;67:429–46.

[15] Lyulin OM. Determination of parameters of spectral lines from several absorption spectra with the MultiSpectrum Fitting computer code**.** Atmos Oceanic Opt 2015;28:487–95.

[16] Jacquemart D, Mandin JY, Dana V, Régalia-Jarlot L, Thomas X, Von der Heyden P. Multispectrum fitting of line parameters for 5μm-cold bands of acetylene. J Quant Spectrosc Radiat Transfer 2002;75:397–422.

[17] Gamache RR, Roller C, Lopes E, Gordon IE, et al. Total internal partition sums for 166 isotopologues of 51 molecules important in planetary atmospheres: Application to HITRAN2016 and beyond. J Quant Spectrosc Radiat Transfer 2017;203:70–87.

[18] Perevalov VI, Lukashevskaya AA. Parameterization of the Effective Dipole Moment Matrix Elements in the Case of the Asymmetric Top Molecules. Application to NO_2 Molecule. Atmospheric and Oceanic Optics 2015;28:17–23.

[19] Jacquemart D, Lacome N, Mandin JY. Line intensities of $^{12}C_2H_2$ in the1.3, 1.2, and 1 μm spectral regions. J Quant Spectrosc Radiat Transfer 2009;110:733–742.

[20] Kassi S, Lyulin OM, Béguier S, Campargue A. New assignments and a rare peculiarity in the high sensitivity CRDS spectrum of acetylene near 8000 cm^{-1}. J Mol Spectrosc 2016;326:106-114.

[21] Weber M, Blass WE, Halsey GW, Hillman JJ, and Maguire WC. ℓ-Resonance effects in the ν_5, $2\nu_5$-ν_5, and ν_4+ν_5-ν_4 bands of C_2H_2 and $^{13}C^{12}CH_2$ near 13.7 μm. Spectrochim. Acta 48A, 1203-1226 (1992).

[22] Hillman JJ, Jennings DE, Halsey GW, Nadler S, and Blass WE. An Infrared Study of the Bending Region of Acetylene. J Mol Spectrosc 1991;146:389-401.

[23] Jacquemart D, Mandin JY, Dana V, Régalia-Jarlot L, Plateaux JJ, Décatoire D, Rothman LS. The spectrum of acetylene in the 5μm region from new line parameter measurements. J Quant Spectrosc Radiat Transfer 2003:76;237-67.

[24] Rothman LS, Jacquemart D, Barbe A, Chris Benner D et al. The *HITRAN* 2004 molecular spectroscopic database. J Quant Spectrosc Radiat Transfer 2005;96:139–204.

[25] Di Lonardo G, Baldan A, Bramati G, Fusina L. The Infrared Spectrum of $^{12}C^{13}CH_2$: The Bending States up to $\nu_4 + \nu_5 = 4$. J Mol Spectrosc 202;213:57–63.

[26] Chubb KL, Tennyson J, Yurchenko SN. ExoMol molecular line lists – XXXVII. Spectra of acetylene. Monthly notices of the Royal Astronomical Society 2020;493:1531-45.

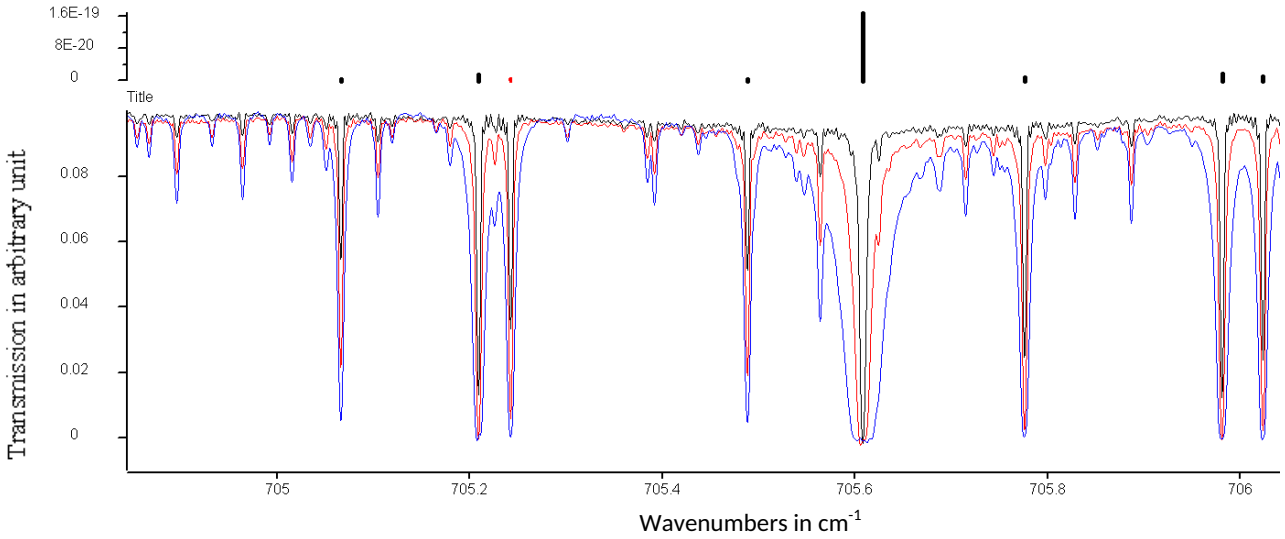

Fig. 1. Spectral range around 705-706 cm^{-1}. Upper panel is a stick plot of HITRAN 2016 [11] for $^{12}C_2H_2$ (black sticks) and $^{12}C^{13}CH_2$ (red sticks). The line intensities (in log scale) are in cm^{-1}/(molecule.cm^{-2}). In the lower panel the 3 experimental spectra are plotted (see experimental conditions in Table 1).

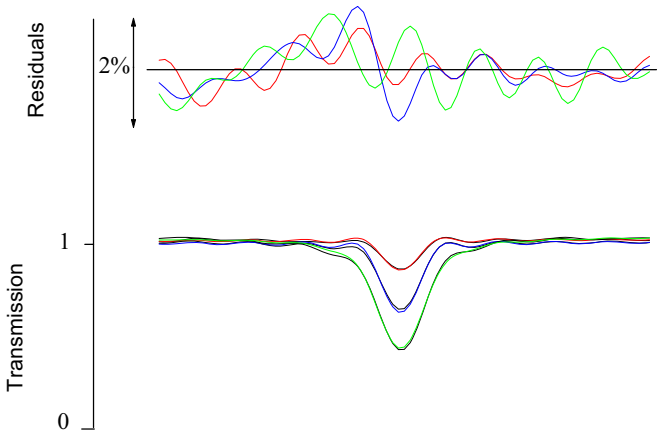

Fig. 2. Simultaneous fit of the P_{ee} (24) transition of the 00002 0 2 – 00001 0 1 band ($2\nu_5^2 - \nu_5^1$) between 675.809 and 675.849 cm^{-1}. In the lower panel are plotted the measured spectra #1-3 (in black) and the respective simulated spectra (red for spectrum #1, blue for # 2, green for #3) using multispectrum fitting procedure. In the upper panel are given the residuals of the fit where the same set of colors been used.

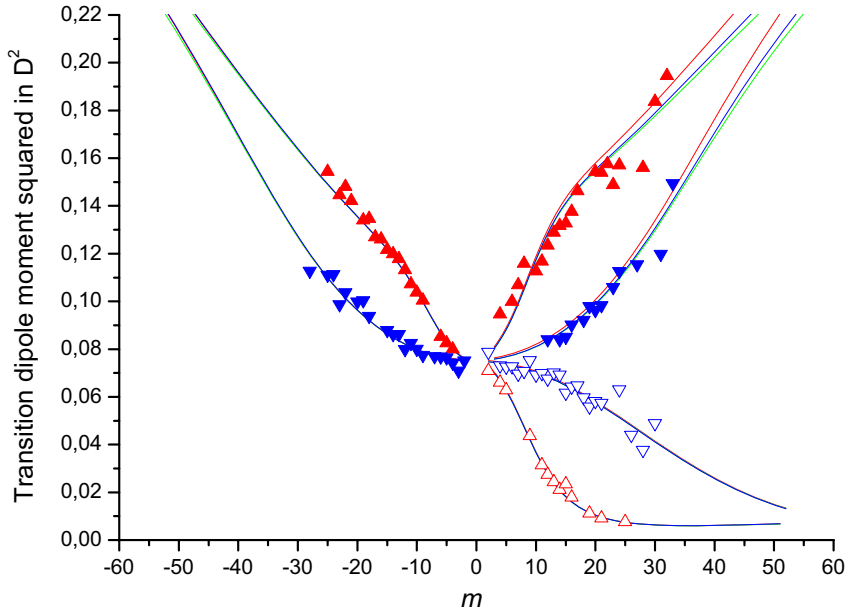

Fig. 3. Transition dipole moment squared of transitions belonging to the P_{ee}, R_{ee} ,P_{ff}, R_{ff}, Q_{ef} and Q_{fe}-branches of the 00021 2-1 – 00020 2 0 band plotted versus m (m = –J, J, J+1 for P, Q, R branch respectively). Triangles are measurements from the present work (open for Q-branch and solid for P-and R-branches). Red triangles are for P_{ee}, R_{ee} and Q_{fe}-branches whereas blue triangles are for P_{ff}, R_{ff} and Q_{ef}-branches. Calculations obtained using parameters of effective dipole moment are in blue line when using parameters from Ref. [4], in green line when using parameters from Ref. [1], and in red line when using parameters from this work (see Table 4).

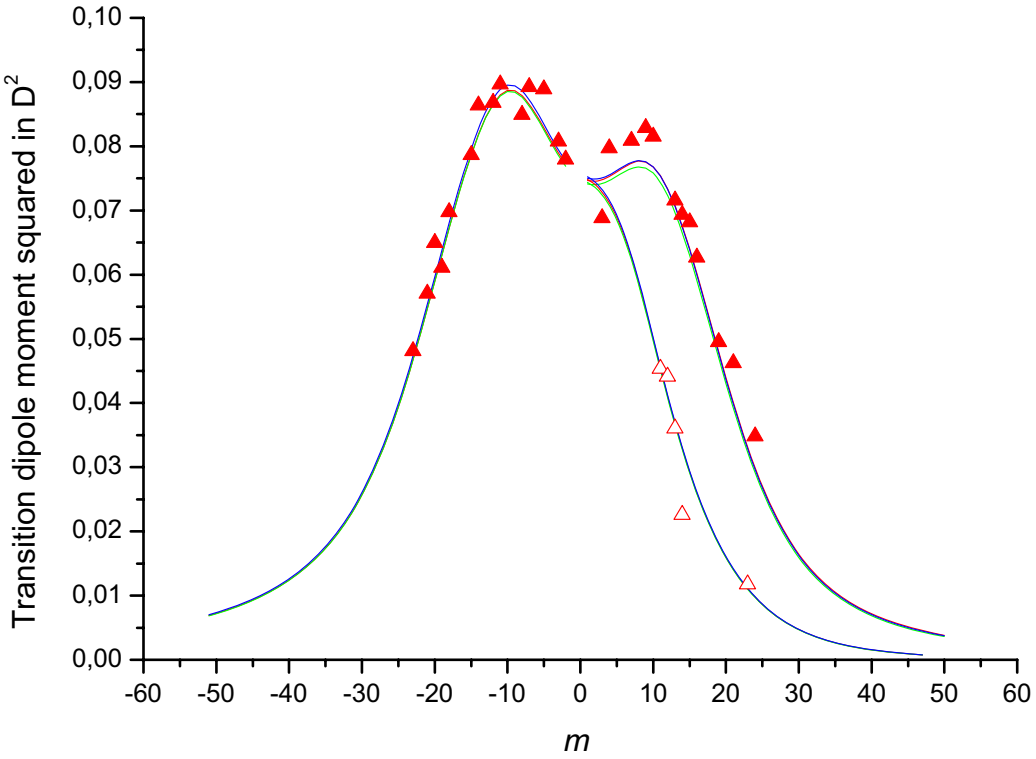

Fig. 4. Transition dipole moment squared of transitions belonging to the P_{ee}, R_{ee} and Q_{fe}-branches of the 00021 0 1 – 00020 0 0 band plotted versus m (m = –J, J, J+1 for P, Q, R branch respectively) Red triangles are measurements from this work for the P_{ee}, R_{ee} and Q_{fe}-branches (open triangles for Q-branch and solid ones for P-and R-branches). Calculations obtained using parameters of effective dipole moment are in blue line when using parameters from Ref. [4], in green line when using parameters from Ref. [1], and in red line when using parameters from this work (see Table 4).

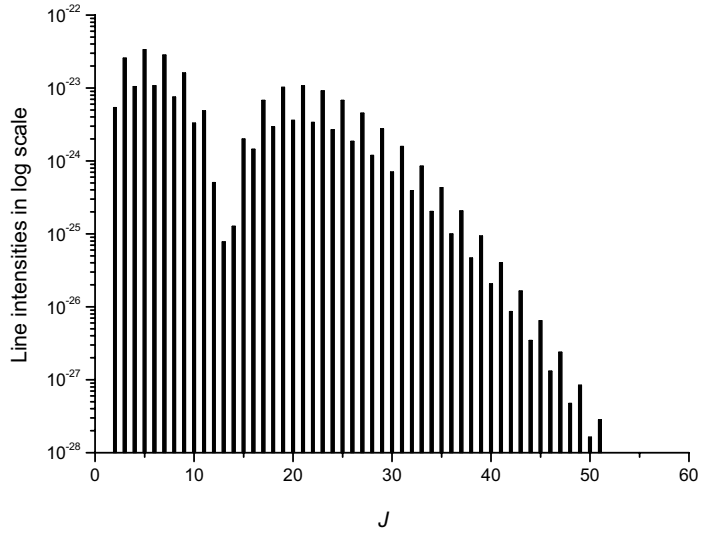

Fig. 5. Calculated line intensities (in $cm^{-1}/(molecule.cm^{-2})$ at 296K) of transitions belonging to the Q_{fe} branch of the 00031 1 1 – 00030 1 0 band plotted versus *J*.

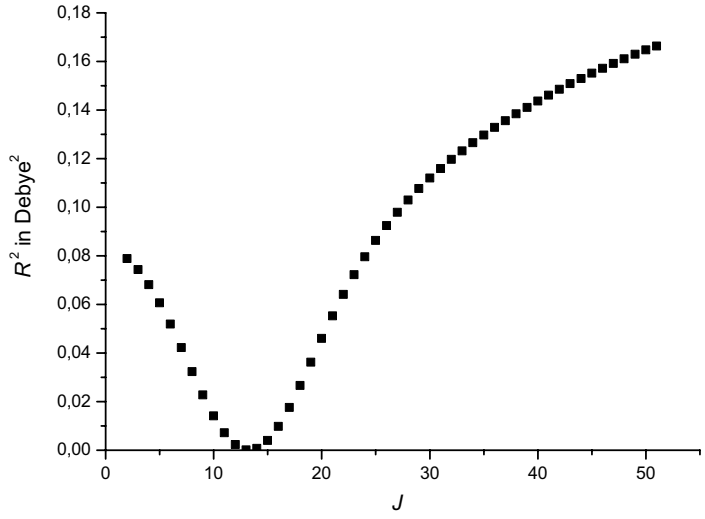

Fig. 6. Calculated transition dipole moment squared of transitions belonging to the Q_{fe} branch of the 00031 1 1 – 00030 1 0 band plotted versus *J*.

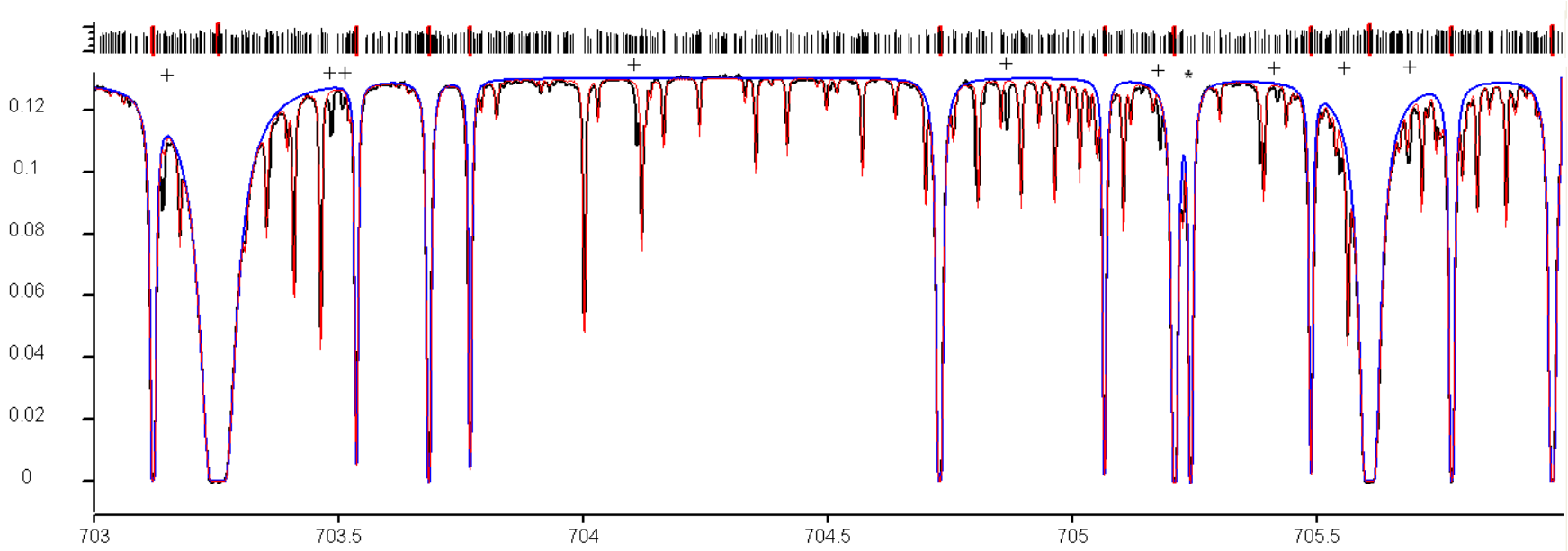

Fig.7. Synthetic spectra between 703 and 706 cm^{-1} using HITRAN 2016 or line list of this work. On the top in the first panel are plotted the transitions of $^{12}C_2H_2$ from HITRAN2016 (red stick) and from the recommended line list of this work (black stick). In the main panel, experimental spectrum recorded at 9.3 matm of natural C_2H_2 is plotted in black. Synthetic spectra are plotted in blue (HITRAN 2016) and red (recommended line list + HITRAN2016 for $^{12}C^{13}C_2H_2$ transitions). The star symbol corresponds to the only $^{12}C^{13}C_2H_2$ transition present in HITRAN 2016 in the plotted spectral range. The + symbols correspond to missing $^{12}C^{13}C_2H_2$ transitions assigned from the work of Di Lonardo et al. [25].

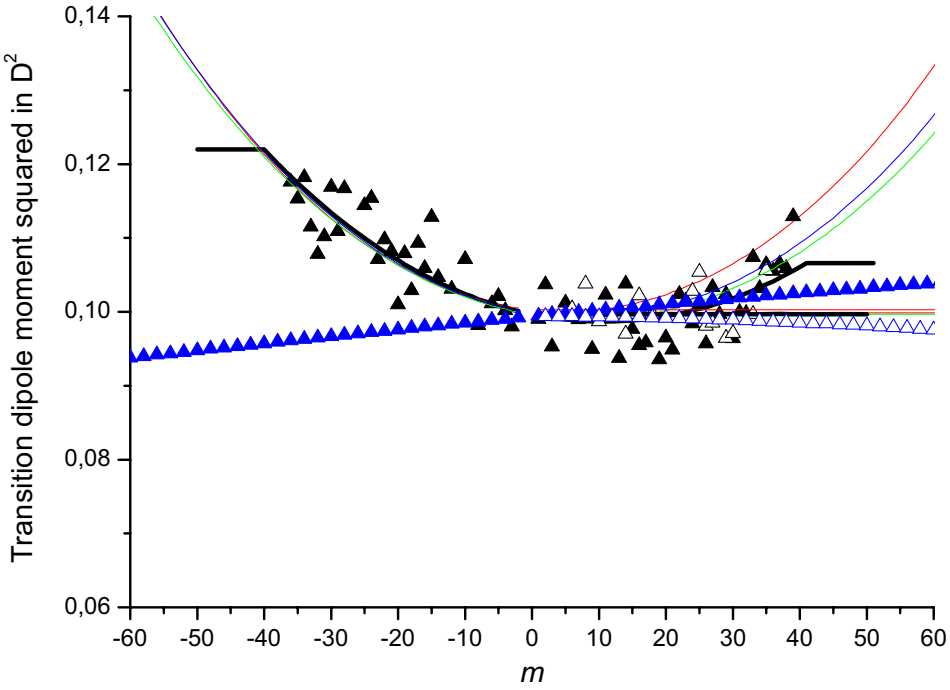

Fig. 8. Transition dipole moment squared of transitions belonging to the P_{ee}, R_{ee} and Q_{fe}-branches of the 00001 0 1 – 00000 0 0 band (ν_5^1) plotted versus m ($m = -J, J, J+1$ for P, Q, R branch respectively). Black line is from HITRAN [11]. Black triangles are measurements from Ref. [14] (open for Q-branch and solid for P-and R-branches). Calculations obtained using parameters of effective dipole moment are in blue line when using parameters from Ref. [4], in green line when using parameters from Ref. [1], and in red line when using parameters from this work (see Table 4). Plotted in blue symbols (open triangles for Q branch and solid triangles for P and R branches) are transition dipole moment squared from EXOMOL [26].

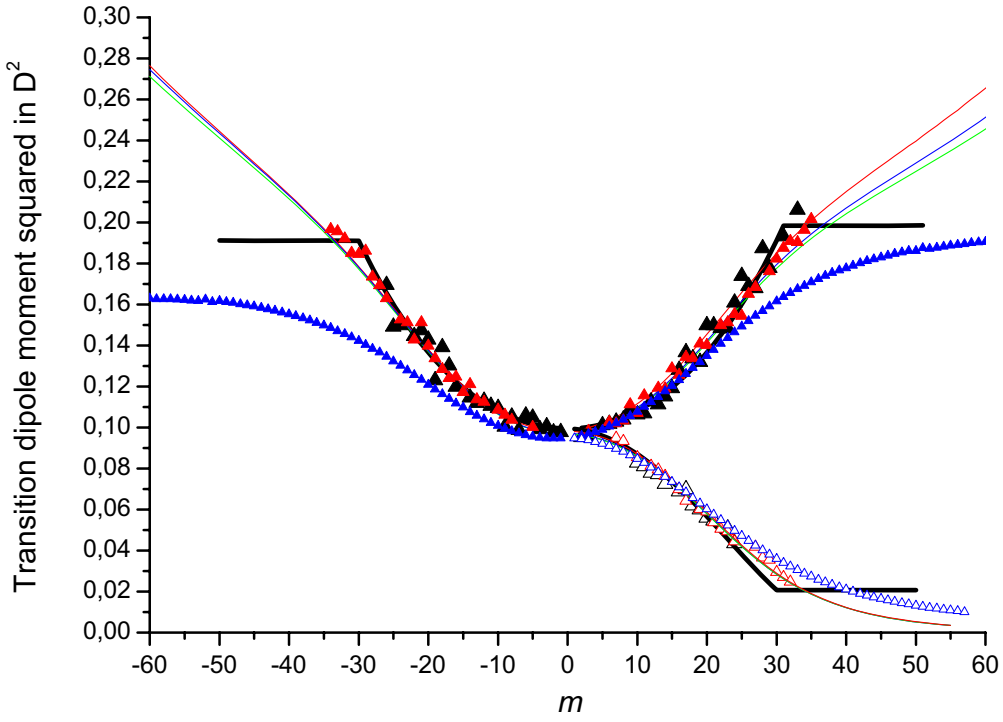

Fig. 9. Transition dipole moment squared of transitions belonging to the P_{ee}, R_{ee} and Q_{fe}-branches of the 00002 0 0 – 00001 0 1 band ($2\nu_5^0 - \nu_5^1$) plotted versus m ($m = -J, J, J+1$ for P, Q, R branch respectively). Black line is from HITRAN [11]. Black and red triangles are measurements from Ref. [13] and the present work respectively (open for Q-branch and solid for P-and R-branches). Calculations obtained using parameters of effective dipole moment are in blue line when using parameters from Ref. [4], in green line when using parameters from Ref. [1], and in red line when using parameters from this work (see Table 4). Plotted in blue symbols (open triangles for Q branch and solid triangles for P and R branches) are transition dipole moment squared from EXOMOL [26].

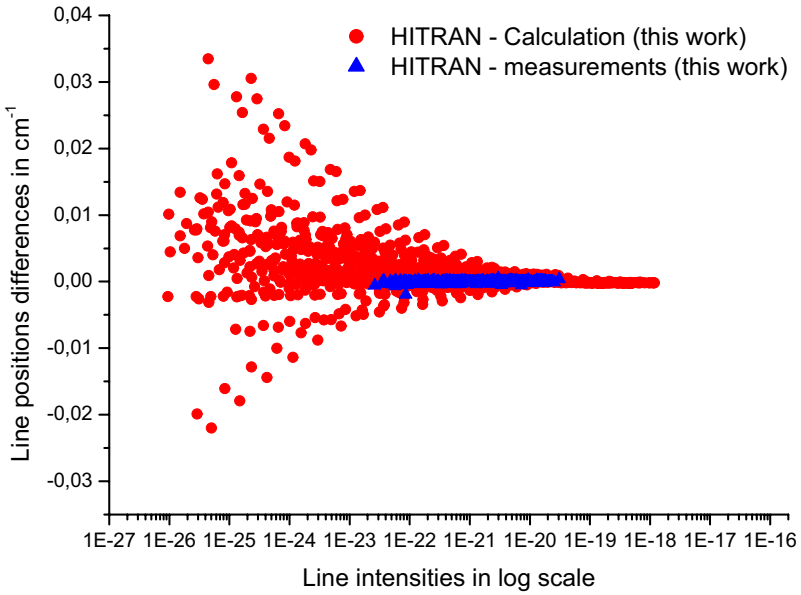

Fig. 10. Line positions differences (HITRAN – Calculation (this work)) in red circles and (HITRAN – measurements (this work)) in blue triangles plotted versus line intensities (in $cm^{-1}/(molecule.cm^{-2})$ at 296K) in a log-scale.

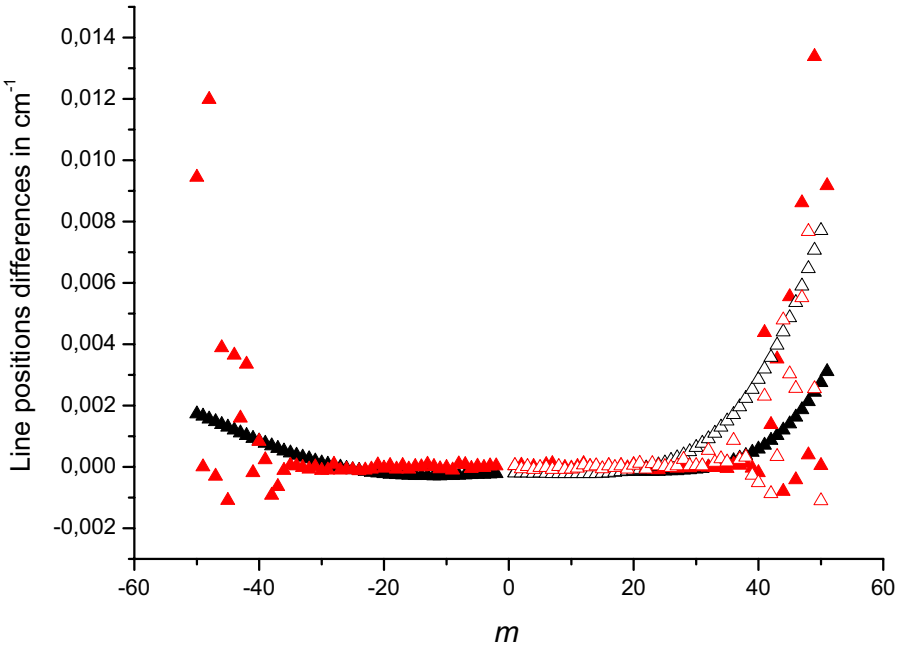

Fig. 11. Line positions differences plotted versus m (m = –J, J, J+1 for P, Q, R branch respectively) for the 00001 0 1 – 00000 0 0 band (ν_5^1). (HITRAN – Calculation (this work)) and (HITRAN – EXOMOL) are plotted in black and red symbols respectively. Solid up-triangles correspond to P_{ee} and R_{ee}-branches, open up-triangles for Q_{fe}-branch.

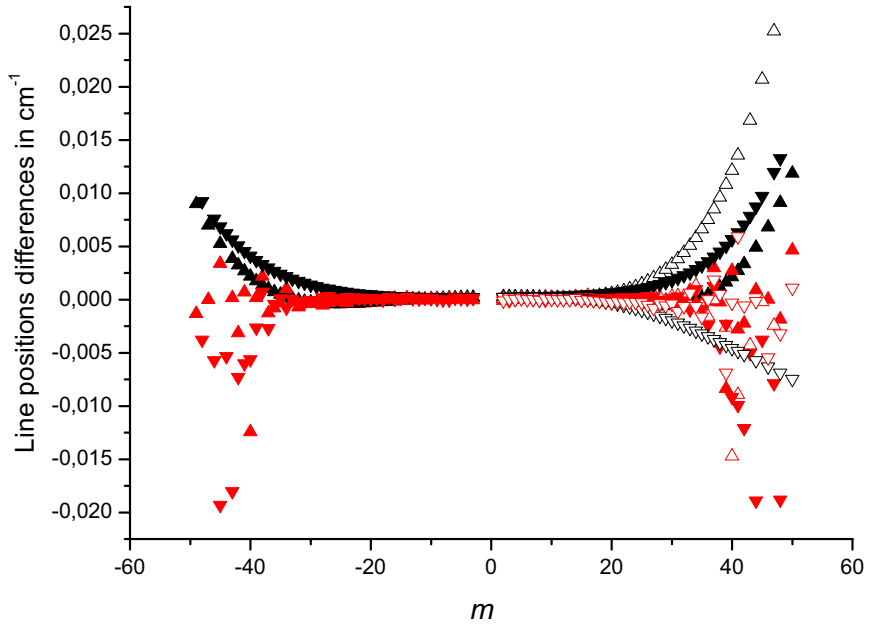

Fig. 12. Line positions differences plotted versus m (m = –J, J, J+1 for P, Q, R branch respectively) for the 00011 1 1 – 00010 1 0 band. (HITRAN – Calculation (this work)) and (HITRAN – EXOMOL) are plotted in black and red symbols respectively. Solid up-triangles correspond to P_{ee} and R_{ee}-branches, solid down-triangles to P_{ff} and R_{ff}-branches, and open up- and down-triangles to Q_{fe}- and Q_{ef}-branches respectively.

Table 1: Experimental conditions and characteristics of the recorded spectra.

Commercial sample (Air Liquide Alphagaz)	
Natural C_2H_2	97.760% of $^{12}C_2H_2$
Stated purity	99.55%
Total absorption path	25.7(1) cm
Collimator focal length	418 mm
Radius of the iris	1.0 mm

Spectrum number	Total pressure (matm)	Temperature (K)	Bruker-resolution[a] (cm^{-1})	Number of co-added scans
1	2.396	294.0	0.004	598
2	4.916	294.5	0.004	600
3	9.319	294.3	0.004	600

[a] Bruker-resolution = $0.9/\Delta_{max}$. Δ_{max} being the maximum optical path difference.

Table 2. Measurements of line positions (σ_{Obs} in cm^{-1}) and intensities (S_{Obs} in $cm^{-1}/(molecule.cm^{-2})$ at 296K in natural abundances) for the $2\nu_5^0 - \nu_5^1$ band.

Assignment	σ_{Obs}	S_{Obs}	m	R^2_{Obs}	E_{low}
Pee 5 00002 0 0-00001 0 1	708.28858	0.495E-20	-5	0.1002	764.4459
Pee 8 00002 0 0-00001 0 1	701.39660	0.179E-19	-8	0.1036	813.8495
Pee 9 00002 0 0-00001 0 1	699.11600	0.611E-20	-9	0.1062	835.0207
Pee 10 00002 0 0-00001 0 1	696.84314	0.183E-19	-10	0.1086	858.5430
Pee 12 00002 0 0-00001 0 1	692.31842	0.171E-19	-12	0.1125	912.6394
Pee 13 00002 0 0-00001 0 1	690.06549	0.534E-20	-13	0.1137	943.2125
Pee 14 00002 0 0-00001 0 1	687.81789	0.155E-19	-14	0.1211	976.1350
Pee 15 00002 0 0-00001 0 1	685.57511	0.448E-20	-15	0.1172	1011.4062
Pee 16 00002 0 0-00001 0 1	683.33634	0.126E-19	-16	0.1247	1049.0256
Pee 17 00002 0 0-00001 0 1	681.10089	0.363E-20	-17	0.1241	1088.9926
Pee 18 00002 0 0-00001 0 1	678.86797	0.967E-20	-18	0.1285	1131.3064
Pee 19 00002 0 0-00001 0 1	676.63694	0.283E-20	-19	0.1336	1175.9664
Pee 20 00002 0 0-00001 0 1	674.40696	0.739E-20	-20	0.1398	1222.9719
Pee 21 00002 0 0-00001 0 1	672.17749	0.219E-20	-21	0.1512	1272.3220
Pee 22 00002 0 0-00001 0 1	669.94754	0.502E-20	-22	0.1428	1324.0159
Pee 23 00002 0 0-00001 0 1	667.71685	0.142E-20	-23	0.1512	1378.0529
Pee 24 00002 0 0-00001 0 1	665.48463	0.339E-20	-24	0.1527	1434.4319
Pee 26 00002 0 0-00001 0 1	661.01393	0.216E-20	-26	0.1630	1554.2123
Pee 27 00002 0 0-00001 0 1	658.77469	0.569E-21	-27	0.1693	1617.6118
Pee 28 00002 0 0-00001 0 1	656.53234	0.131E-20	-28	0.1735	1683.3492
Pee 29 00002 0 0-00001 0 1	654.28685	0.347E-21	-29	0.1862	1751.4240
Pee 30 00002 0 0-00001 0 1	652.03790	0.754E-21	-30	0.1846	1821.8344
Pee 31 00002 0 0-00001 0 1	649.78546	0.182E-21	-31	0.1851	1894.5793
Pee 32 00002 0 0-00001 0 1	647.52967	0.404E-21	-32	0.1921	1969.6580
Pee 33 00002 0 0-00001 0 1	645.27053	0.967E-22	-33	0.1957	2047.0688
Pee 34 00002 0 0-00001 0 1	643.00773	0.203E-21	-34	0.1967	2126.8105
Qef 7 00002 0 0-00001 0 1	719.95309	0.308E-19	7	0.09491	795.2927
Qef 8 00002 0 0-00001 0 1	719.94919	0.105E-19	8	0.09340	814.1874
Qef 10 00002 0 0-00001 0 1	719.93421	0.949E-20	10	0.08541	859.0591
Qef 12 00002 0 0-00001 0 1	719.90662	0.826E-20	12	0.08126	913.3709
Qef 13 00002 0 0-00001 0 1	719.88652	0.225E-19	13	0.07947	944.0658
Qef 14 00002 0 0-00001 0 1	719.86137	0.659E-20	14	0.07624	977.1193
Qef 16 00002 0 0-00001 0 1	719.79273	0.481E-20	16	0.06974	1050.3000
Qef 17 00002 0 0-00001 0 1	719.74779	0.116E-19	17	0.06429	1090.4258
Qef 19 00002 0 0-00001 0 1	719.63261	0.792E-20	19	0.06020	1177.7453
Qef 20 00002 0 0-00001 0 1	719.56104	0.216E-20	20	0.05887	1224.9374
Qef 21 00002 0 0-00001 0 1	719.47910	0.487E-20	21	0.05376	1274.4834
Qef 22 00002 0 0-00001 0 1	719.38625	0.124E-20	22	0.05060	1326.3824
Qef 23 00002 0 0-00001 0 1	719.28190	0.291E-20	23	0.04927	1380.6335
Qef 24 00002 0 0-00001 0 1	719.16548	0.691E-21	24	0.04436	1437.2359
Qef 27 00002 0 0-00001 0 1	718.73992	0.897E-21	27	0.04182	1621.1406
Qef 28 00002 0 0-00001 0 1	718.57184	0.196E-21	28	0.03653	1687.1379
Qef 29 00002 0 0-00001 0 1	718.38992	0.424E-21	29	0.03537	1755.4812
Qef 30 00002 0 0-00001 0 1	718.19631	0.864E-22	30	0.02954	1826.1693
Qef 31 00002 0 0-00001 0 1	717.98538	0.171E-21	31	0.02695	1899.2012
Qef 32 00002 0 0-00001 0 1	717.76295	0.374E-22	32	0.02467	1974.5755
Ree 2 00002 0 0-00001 0 1	727.07335	0.573E-20	3	0.09818	736.2127
Ree 5 00002 0 0-00001 0 1	734.26923	0.440E-20	6	0.01026	764.4459

Ree	6	00002	0	0-00001	0	1	736.68432	0.147E-19	7	0.01020	778.5618
Ree	7	00002	0	0-00001	0	1	739.10696	0.538E-20	8	0.01034	795.0298
Ree	8	00002	0	0-00001	0	1	741.53660	0.182E-19	9	0.01113	813.8495
Ree	9	00002	0	0-00001	0	1	743.97281	0.595E-20	10	0.01071	835.0207
Ree	10	00002	0	0-00001	0	1	746.41480	0.191E-19	11	0.01156	858.5430
Ree	12	00002	0	0-00001	0	1	751.31350	0.184E-19	13	0.01193	912.6394
Ree	13	00002	0	0-00001	0	1	753.76882	0.571E-20	14	0.01189	943.2125
Ree	14	00002	0	0-00001	0	1	756.22700	0.171E-19	15	0.01287	976.1350
Ree	15	00002	0	0-00001	0	1	758.68726	0.504E-20	16	0.01256	1011.4062
Ree	16	00002	0	0-00001	0	1	761.14881	0.144E-19	17	0.01344	1049.0256
Ree	17	00002	0	0-00001	0	1	763.61084	0.420E-20	18	0.01337	1088.9926
Ree	18	00002	0	0-00001	0	1	766.07248	0.115E-19	19	0.01409	1131.3064
Ree	19	00002	0	0-00001	0	1	768.53302	0.324E-20	20	0.01401	1175.9664
Ree	21	00002	0	0-00001	0	1	773.44775	0.242E-20	22	0.01499	1272.3220
Ree	22	00002	0	0-00001	0	1	775.90062	0.598E-20	23	0.01512	1324.0159
Ree	23	00002	0	0-00001	0	1	778.34968	0.165E-20	24	0.01553	1378.0529
Ree	24	00002	0	0-00001	0	1	780.79446	0.392E-20	25	0.01543	1434.4319
Ree	25	00002	0	0-00001	0	1	783.23451	0.110E-20	26	0.01651	1493.1520
Ree	26	00002	0	0-00001	0	1	785.66942	0.261E-20	27	0.01685	1554.2123
Ree	28	00002	0	0-00001	0	1	790.52292	0.158E-20	29	0.01761	1683.3492
Ree	29	00002	0	0-00001	0	1	792.94117	0.406E-21	30	0.01823	1751.4240
Ree	30	00002	0	0-00001	0	1	795.35350	0.924E-21	31	0.01875	1821.8344
Ree	31	00002	0	0-00001	0	1	797.76000	0.228E-21	32	0.01909	1894.5793
Ree	32	00002	0	0-00001	0	1	800.16051	0.491E-21	33	0.01903	1969.6580
Ree	33	00002	0	0-00001	0	1	802.55513	0.120E-21	34	0.01963	2047.0688
Ree	34	00002	0	0-00001	0	1	804.94402	0.259E-21	35	0.02016	2126.8105

Note: For assignment, the branch type is first given, then the *e*/*f* Wang symmetry of the upper and lower state, and finally the rotational quantum number *J* of the lower state. Then are reported the vibrational assignment for the upper and lower states (V_1 V_2 V_3 V_4 V_5 ℓ_4 ℓ_5). Measured line positions (σ_{Meas}) and energies of the lower state (E_{low}) are given in cm^{-1}. The transition dipole moments squared (R^2_{Obs}) are given in debye^2.

Table 3. Summary of measurements performed in this work.

Studied band	$\Delta\ell_4$	$\Delta\ell_5$	N	Positions	Line intensities	J
				min - max	min - max	min - max
00002 0 0 * 00001 0 1	0	-1	74	643.0 - 804.9	3.74E-23 - 3.08E-20	2 - 34
00002 0 2 * 00001 0 1	0	-1	90	651.0 - 819.6	3.55E-23 - 2.36E-20	2 - 37
00011 1-1 * 00010 1 0	0	1	122	638.3 - 806.0	3.70E-23 - 2.55E-20	1 - 35
00011 1 1 * 00010 1 0	0	1	89	657.5 - 812.6	2.64E-23 - 2.31E-20	4 - 34
00012 1 0 00011 1-1	0	1	108	638.3 - 805.3	1.03E-23 - 2.52E-21	0 - 34
00012 1 2 00011 1 1	0	1	60	673.8 - 795.8	4.54E-23 - 1.57E-21	6 - 26
00003 0 1 00002 0 0	0	1	51	660.2 - 784.7	4.39E-23 - 1.75E-21	1 - 29
00003 0 3 00002 0 2	0	1	46	675.3 - 789.7	6.25E-23 - 1.29E-21	6 - 24
00021 0 1 00020 0 0	0	1	31	674.4 - 785.2	6.11E-23 - 1.47E-21	2 - 23
00021 0 1 00020 2 0	-2	1	58	676.3 - 802.1	1.15E-23 - 1.26E-21	2 - 28
00021 2 1 00020 2 0	0	1	81	674.0 - 809.8	1.04E-23 - 1.41E-21	4 - 30
00021 2-1 00020 2 0	0	-1	108	649.5 - 794.5	1.24E-23 - 1.00E-21	2 - 32
00021 2-1 00020 0 0	2	-1	32	673.2 - 754.7	1.11E-23 - 1.16E-21	0 - 27
00012 1 0 00011 1 1	0	-1	47	654.5 - 765.9	4.25E-23 - 4.36E-22	2 - 23
00012-1 2 00011 1-1	-2	3	59	660.8 - 789.3	1.02E-23 - 1.20E-22	1 - 24
00012-1 2 00011 1 1	-2	1	59	668.9 - 779.7	2.71E-23 - 3.92E-22	3 - 26
00003 0 1 00002 0 2	0	-1	68	649.4 - 779.4	1.02E-23 - 5.00E-22	2 - 29
00021 2 1 00020 0 0	2	1	37	662.1 - 815.2	1.15E-23 - 4.63E-22	3 - 35

Note: The band notation refers to the upper and lower vibrational state, see note of Table 2. The line positions are given in cm^{-1} and the line intensities are in $cm^{-1}/(molecule.cm^{-2})$ at 296K in natural abundance. The star marks the bands already measured in Ref. [13] and present in HITRAN and GEISA databases.

Table 4. Effective dipole moment parameters for the $\Delta P=1$ series of transitions.

Parameter [a]	ΔV_1	ΔV_2	ΔV_3	ΔV_4	ΔV_5	$\Delta \ell_4$	$\Delta \ell_5$	*This work*	Ref. [1]	Ref. [4]
M	0	0	0	0	1	0	1	-0.1583(2)	-0.1578(2)	-0.1579(2)
κ_5	0	0	0	0	1	0	1	-0.0131(8)	-0.017(2)	0.013(2)
b_J	0	0	0	0	1	0	1	$-0.49(3) \times 10^{-3}$	$-0.76\ (5) \times 10^{-3}$	$-0.72\ (5) \times 10^{-3}$
d_J	0	0	0	0	1	0	1	$0.51(2) \times 10^{-4}$	$0.45(3) \times 10^{-4}$	$0.47(3) \times 10^{-4}$
M	0	0	0	2	-1	2	-1	$-0.3361(4) \times 10^{-2}$	$-0.3343(5) \times 10^{-2}$	
κ_4	0	0	0	2	-1	2	-1	0.028(4)	0.020(3)	
b_J	0	0	0	2	-1	2	-1	$-0.211(8) \times 10^{-2}$	$-0.244(9) \times 10^{-2}$	
d_J	0	0	0	2	-1	2	-1	$-0.66(5) \times 10^{-4}$	$-0.63(6) \times 10^{-4}$	
M	0	0	0	2	-1	0	1	$0.669(2) \times 10^{-2}$	$0.665(2) \times 10^{-2}$	
κ_4	0	0	0	2	-1	0	1	0.060(2)	0.059(2)	
a_5	0	0	0	2	-1	0	1	0.030(2)	0.026(2)	
b_J	0	0	0	2	-1	0	1	$-0.109(7) \times 10^{-2}$	$-0.119(8) \times 10^{-2}$	
d_J	0	0	0	2	-1	0	1	$-0.55(4) \times 10^{-4}$	$-0.61(4) \times 10^{-4}$	
M	0	0	0	2	-1	-2	3	$-0.36(3) \times 10^{-3}$	$-0.30(3) \times 10^{-3}$	

[a] Parameters M are given in Debye while the other parameters are dimensionless.
[b] Confidence intervals (1 SD, in unit of the last quoted digit) are given between parentheses.

Table 5. Statistics of the fitted bands of the $\Delta P = 1$ series.

Measured bands	Spectral range in cm^{-1}	N [a]	J_{max} [b]	MR [c] in %	RMS [d] in %
Band measured in Ref. [14]					
00001 0 1 - 00000 0 0	644.5-820.2	77	38	-1.10	4.01
Bands measured in Ref. [13]					
00002 0 0 - 00001 0 1	661.0-800.2	64	32	-1.13	3.79
00002 0 2 - 00001 0 1	674.7-794.8	79	30	-1.01	2.67
00011 1-1 - 00010 1 0	655.8-787.5	109	31	-0.13	3.31
00011 1 1 - 00010 1 0	669.4-798.8	98	28	-0.15	4.19
Bands measured in Ref. [1]					
00020 2 0 - 00001 0 1	434.6-564.0	107	33	-1.08	5.82
00020 0 0 - 00001 0 1	429.6-586.8	84	34	1.77	4.72
00030 1 0 - 00011 1 1	449.7-583.9	77	27	-1.08	4.56
00030 1 0 - 00011 1-1	478.9-580.6	37	22	1.41	6.29
00030 3 0 - 00011 1 1	468.3-559.8	40	25	0.85	5.54
00021 0 1 - 00002 0 0	457.4-568.3	33	23	0.93	5.80
00021 0 1 - 00002 0 2	458.6-527.2	52	25	-0.11	3.45
00021 2 1 - 00002 0 2	456.8-555.6	20	21	4.73	8.88
00021 2 1 - 00002 0 0	555.7-565.6	2	21	6.89	6.92
Bands measured in this work					
00002 0 0 - 00001 0 1	643.0-804.9	72	34	-0.13	2.69
00002 0 2 - 00001 0 1	651.0-819.6	87	37	0.48	3.33
00011 1-1 - 00010 1 0	638.3-806.0	119	35	0.27	3.54
00011 1 1 - 00010 1 0	657.5-812.6	85	34	-0.51	3.74
00003 0 1 - 00002 0 0	660.2-784.7	47	29	1.49	3.99
00003 0 1 - 00002 0 2	649.4-779.4	64	29	-1.20	4.48
00003 0 3 - 00002 0 2	675.3-784.7	40	22	-0.95	3.59
00012 1 0 - 00011 1 1	654.5-765.9	46	23	-0.96	4.53
00012 1 0 - 00011 1-1	638.3-795.6	65	34	1.92	4.99
00012 1 2 - 00011 1 1	673.8-795.8	50	26	-0.15	4.46
00012-1 2 - 00011 1 1	668.9-779.7	54	26	2.27	4.29
00012-1 2 - 00011 1-1	652.3-805.3	48	33	3.29	6.72
00021 0 1 - 00020 0 0	674.3-774.0	28	23	3.49	4.72
00021 0 1 - 00020 2 0	676.3-802.1	28	28	6.32	8.16
00021 2 1 - 00020 0 0	662.1-810.6	22	33	0.95	6.06
00021 2 1 - 00020 2 0	674.0-809.8	64	30	0.30	3.86
00021 2-1 - 00020 0 0	673.2-754.7	26	27	-1.42	3.80
00021 2-1 - 00020 2 0	649.5-794.5	99	32	-0.19	3.72

Note: The band notation refers to the upper and lower vibrational states ($V_1\,V_2\,V_3\,V_4\,V_5\,\ell_4\,\ell_5$).

[a] Number of the fitted line intensities for a given band.

[b] Maximum value of the angular momentum quantum number for a given band.

[c] Mean residuals.

[d] Root mean squares of the residuals.

Table 6. Calculation based on parameter of Table 4 (this work) for the Q_{fe} and R_{ee} branches of the 00031 1 1 – 00030 1 0 band. The first column corresponds to the vibrational labeling used for a whole series of transition. Then the type of branch, the Wang symmetry e/f of the upper and lower state, J of lower state, calculated line positions in cm^{-1}, calculated line intensities at 296K for natural abundances in $cm^{-1}/(molecule.cm^{-2})$, the lower state energy cm^{-1}, then, for upper and lower levels, the two main contributors to the eigenfunctions (with percentages, see text). A star at the beginning of the line means that the main contributors to the eigenfunctions are different from the vibrational labeling used for a whole series of transition.

	Vibrational labeling of the band	Br	J	Position	Intensity	E_{Low}	Upper main contributors First	per	Second	per	Lower main contributors First	per	Second	per
	...													
	00031 1 1-00030 1 0	Qfe	14	731.74096	1.272E-25	2101.70012	00031 1 1	46%	00031 1-1	26%	00030 1 0	88%	00030 3 0	11%
	00031 1 1-00030 1 0	Qfe	15	731.87770	2.005E-24	2137.05022	00031 1 1	39%	00031 1-1	28%	00030 1 0	84%	00030 3 0	14%
	00031 1 1-00030 1 0	Qfe	16	732.00377	1.449E-24	2174.76900	00031 1 1	33%	00031 1-1	31%	00030 1 0	81%	00030 3 0	18%
*	00031 1 1-00030 1 0	Qfe	17	732.11764	6.793E-24	2214.85691	00031 1-1	32%	00031 3 1	30%	00030 1 0	77%	00030 3 0	22%
*	00031 1 1-00030 1 0	Qfe	18	732.21895	2.949E-24	2257.31374	00031 3 1	35%	00031 1-1	34%	00030 1 0	73%	00030 3 0	26%
*	00031 1 1-00030 1 0	Qfe	19	732.30829	1.022E-23	2302.13864	00031 3 1	39%	00031 1-1	35%	00030 1 0	69%	00030 3 0	30%
*	00031 1 1-00030 1 0	Qfe	20	732.38697	3.613E-24	2349.33035	00031 3 1	42%	00031 1-1	35%	00030 1 0	65%	00030 3 0	34%
*	00031 1 1-00030 1 0	Qfe	21	732.45667	1.076E-23	2398.88729	00031 3 1	45%	00031 1-1	36%	00030 1 0	62%	00030 3 0	37%
*	00031 1 1-00030 1 0	Qfe	22	732.51925	3.381E-24	2450.80772	00031 3 1	48%	00031 1-1	36%	00030 1 0	59%	00030 3 0	40%
*	00031 1 1-00030 1 0	Qfe	23	732.57660	9.170E-24	2505.08983	00031 3 1	50%	00031 1-1	36%	00030 1 0	56%	00030 3 0	43%
	...													
	00031 1 1-00030 1 0	Ree	23	787.55801	2.763E-25	2505.08983	00031 1 1	47%	00031 3 1	39%	00030 1 0	56%	00030 3 0	43%
	00031 1 1-00030 1 0	Ree	24	789.80567	4.481E-26	2561.73183	00031 1 1	46%	00031 3 1	41%	00030 1 0	53%	00030 3 0	46%
	00031 1 1-00030 1 0	Ree	25	792.04317	5.871E-26	2620.73195	00031 1 1	44%	00031 3 1	42%	00030 1 0	51%	00030 3 0	48%
*	00031 1 1-00030 1 0	Ree	26	794.27160	7.192E-27	2682.08846	00031 3 1	44%	00031 1 1	43%	00030 3 0	50%	00030 1 0	49%
*	00031 1 1-00030 1 0	Ree	27	796.49193	5.664E-27	2745.79968	00031 3 1	45%	00031 1 1	41%	00030 3 0	52%	00030 1 0	47%
*	00031 1 1-00030 1 0	Ree	28	798.70503	1.744E-28	2811.86399	00031 3 1	46%	00031 1 1	40%	00030 3 0	53%	00030 1 0	45%
*	00031 1 1-00030 1 0	Ree	29	800.91165	2.012E-28	2880.27978	00031 3 1	47%	00031 1 1	38%	00030 3 0	55%	00030 1 0	44%
*	00031 1 1-00030 1 0	Ree	30	803.11247	5.125E-28	2951.04548	00031 3 1	48%	00031 1 1	37%	00030 3 0	56%	00030 1 0	43%
*	00031 1 1-00030 1 0	Ree	31	805.30808	3.021E-27	3024.15952	00031 3 1	49%	00031 1 1	36%	00030 3 0	57%	00030 1 0	41%
*	00031 1 1-00030 1 0	Ree	32	807.49901	1.353E-27	3099.62035	00031 3 1	50%	00031 1 1	35%	00030 3 0	58%	00030 1 0	40%
*	00031 1 1-00030 1 0	Ree	33	809.68572	4.524E-27	3177.42640	00031 3 1	51%	00031 1 1	34%	00030 3 0	59%	00030 1 0	39%

Note: The vibrational labeling $V_1\,V_2\,V_3\,V_4\,V_5\,\ell_4\,\ell_5$ is used for upper and lower state.

Table 7. Summary of calculation for the 30 first strongest bands in the $\Delta P = 1$ series of bands. The first column corresponds to the vibrational labeling used for series of transitions (bands). *N* is the total number of transitions belonging to band. Minimum and maximum wavenumbers of calculated transitions belonging to the band are given in cm^{-1}, *Sum_S* is the sum of calculated line intensities (see text) in $cm^{-1}/(molecule.cm^{-2})$ at 296K for natural abundances. *Smin* and *Smax* are respectively the minimum and maximum calculated line intensities in the band. Minimum and maximum values of *J* in the band are given.

	Vibrational labeling of the band		*N*	Wavenumbers min – max	*Sum_S*	*Smin*	*Smax*	*J* min	*J* max	
H	00001 0 1	00000 0 0	195	577.0-881.5	2.46E-17	1.36E-28	1.18E-18	0	65	Obs
H	00002 0 2	00001 0 1	343	589.8-887.6	6.94E-19	1.32E-28	3.59E-20	1	61	Obs
H	00002 0 0	00001 0 1	176	583.5-869.8	6.89E-19	1.40E-28	3.01E-20	1	62	Obs
H	00011 1 1	00010 1 0	345	588.7-892.7	6.33E-19	1.09E-28	3.18E-20	1	62	Obs
H	00011 1-1	00010 1 0	355	579.9-866.0	6.23E-19	1.08E-28	3.11E-20	1	61	Obs
	00003 0 1	00002 0 0	167	585.7-853.8	4.07E-20	1.07E-28	1.87E-21	0	57	Obs
*	00021 0 1	00020 0 0	149	604.2-846.0	3.62E-20	1.13E-28	1.80E-21	0	51	Obs
	00012 1 2	00011 1 1	315	603.8-871.6	3.49E-20	1.00E-28	1.63E-21	2	58	Obs
	00003 0 3	00002 0 2	313	598.9-868.5	2.89E-20	1.02E-28	1.36E-21	2	57	Obs
*	00012 1 0	00011 1-1	319	587.1-854.9	2.79E-20	1.01E-28	2.54E-21	0	58	Obs
*	00012-1 2	00011 1-1	302	601.6-862.4	2.69E-20	1.18E-28	2.54E-21	0	57	Obs
*	00021 2 1	00020 2 0	282	627.2-881.0	2.58E-20	1.01E-28	1.40E-21	2	54	Obs
*	00021 2-1	00020 2 0	321	582.9-853.7	2.26E-20	1.10E-28	1.02E-21	2	57	Obs
	00021 2-1	00020 0 0	126	630.2-798.0	1.49E-20	1.16E-28	1.20E-21	0	53	Obs
*	00021 0 1	00020 2 0	310	612.6-879.5	1.27E-20	1.25E-28	1.46E-21	2	57	Obs
*	00021 2 1	00020 0 0	162	600.1-865.0	1.05E-20	1.06E-28	4.70E-22	2	57	Obs
	00003 0 1	00002 0 2	298	590.2-854.8	9.41E-21	1.02E-28	5.07E-22	2	56	Obs
*	00012-1 2	00011 1 1	307	594.9-859.1	8.56E-21	1.25E-28	3.92E-22	2	57	Obs
*	00012 1 0	00011 1 1	297	578.7-843.6	8.46E-21	1.01E-28	4.44E-22	2	53	Obs
	01001 0 1	01000 0 0	151	608.3-847.6	1.69E-21	1.15E-28	8.11E-23	0	51	
*	00022 0 0	00021 0 1	143	620.0-838.9	1.65E-21	1.19E-28	8.28E-23	1	51	
*	00022 2 2	00021 2 1	277	616.6-854.1	1.64E-21	1.34E-28	9.87E-23	3	51	
	00022 2-2	00021 2-1	297	590.6-839.7	1.64E-21	1.08E-28	8.05E-23	1	52	
*	00022 0 2	00021 0 1	284	621.7-854.5	1.45E-21	1.05E-28	7.59E-23	1	52	
	00013 1 3	00012 1 2	278	619.9-855.5	1.42E-21	1.11E-28	8.36E-23	3	52	
*	00013 1 1	00012 1 0	282	598.9-855.5	1.35E-21	1.07E-28	7.41E-23	1	52	
*	00031 1-1	00030 1 0	254	598.1-840.2	1.27E-21	1.05E-28	1.02E-22	1	51	
*	00013-1 3	00012-1 2	280	609.4-844.8	1.27E-21	1.12E-28	6.78E-23	1	51	
	00004 0 0	00003 0 1	146	597.2-837.8	1.18E-21	1.18E-28	5.00E-23	1	52	
*	00031 3-1	00030 3 0	283	590.6-837.0	1.18E-21	1.05E-28	5.09E-23	3	52	

Note: The vibrational labeling for upper and lower state corresponds to $V_1\,V_2\,V_3\,V_4\,V_5\,\ell_4\,\ell_5$. A star at the beginning of the line means that the main contributor to the eigenfunctions of the upper or lower states (or both) is changed within the series of transitions (bands). Letter H shows bands present in HITRAN2016 [11]. In the last column "Obs" means that the band was measured in this work or reported in literature (see Section 2).

Declaration of interests

 The authors declare that they have no known competing financial interests or personal relationships that could have appeared to influence the work reported in this paper.

The authors declare the following financial interests/personal relationships which may be considered as potential competing interests:

David Jacquemart: Visualization, Analysis, Investigation, Methodology, Data Curation, Writing - Original Draft. **Pascale Soulard**: Investigation. **Oleg Lyulin**: Methodology, Software, Validation, Formal analysis, Data Curation, Writing - Original Draft.

Supplementary material 2:

Comparisons of R^2 experimental values with R^2 values from HITRAN/EXOMOL/Global model [1,4,present work].

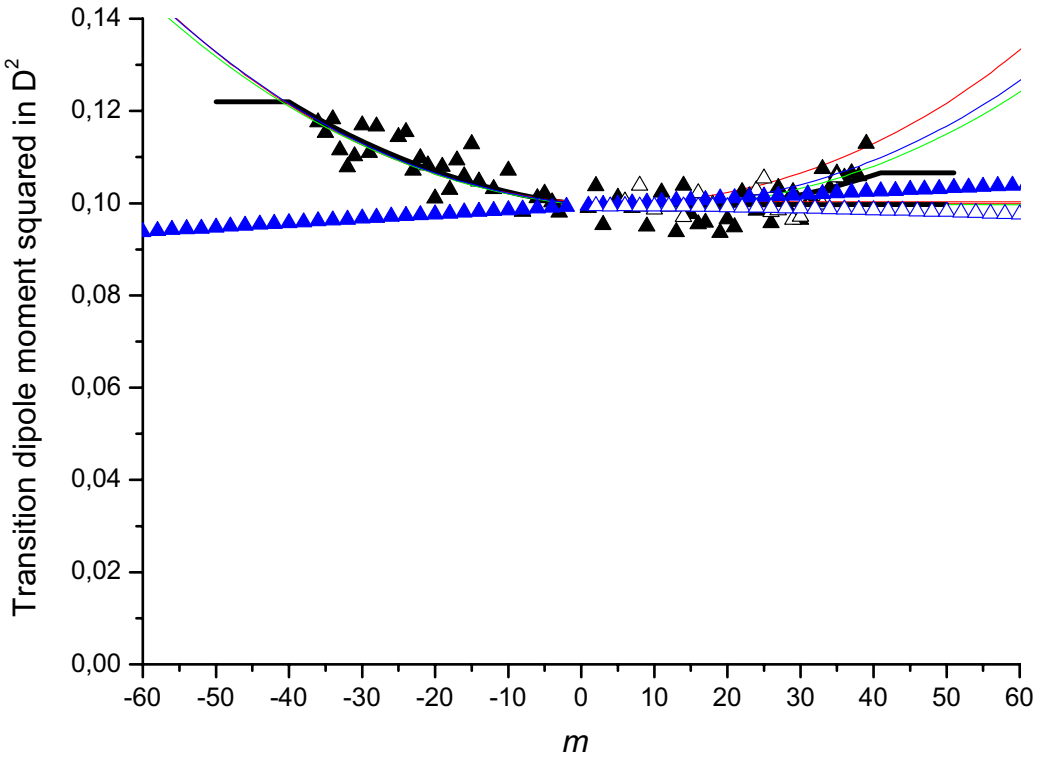

Transition dipole moment squared of transitions belonging to the P_{ee}, R_{ee} and Q_{fe}-branches of the 00001 0 1 – 00000 0 0 band (ν_5^1) plotted versus m. Black line is from HITRAN [11]. Black triangles are measurements from Ref. [14] (open for Q-branch and solid for P-and R-branches). Calculations obtained using parameters of effective dipole moment are in blue line when using parameters from Ref. [4], in green line when using parameters from Ref. [1], and in red line when using parameters from this work (see Table 4). Plotted in blue symbols (open triangles for Q branch and solid triangles for P and R branches) are transition dipole moment squared from EXOMOL [26].

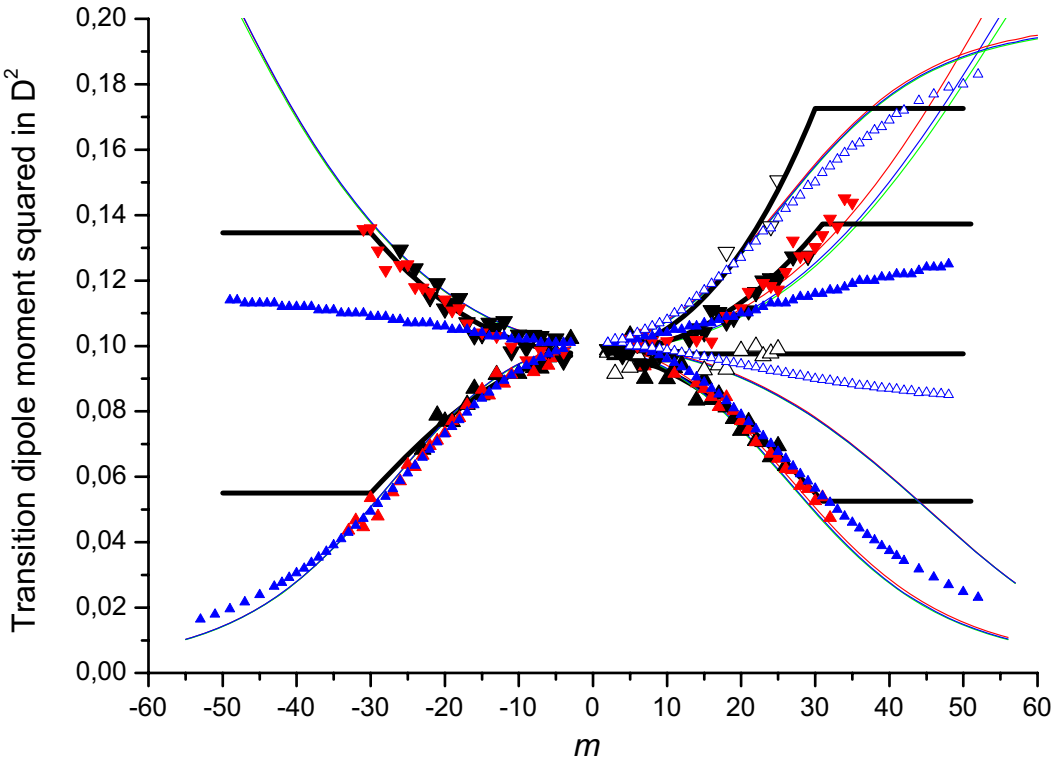

Transition dipole moment squared of transitions belonging to the P_{ee}, R_{ee} ,P_{ff}, R_{ff}, Q_{ef} and Q_{fe}-branches of the **00011 1 1 – 00010 1 0** band plotted versus m (noted $(\nu_4+\nu_5)^2 - \nu_4^1$) in Ref. [13] as well as in HITRAN and GEISA databases). Black line is from HITRAN [11]. Black and red triangles are measurements from Ref. [13] and the present work respectively (open for Q-branch and solid for P-and R-branches). Upside triangles are for P_{ee}, R_{ee} and Q_{fe}-branches whereas downside triangles are for P_{ff}, R_{ff} and Q_{ef}-branches. Calculations obtained using parameters of effective dipole moment are in blue line when using parameters from Ref. [4], in green line when using parameters from Ref. [1], and in red line when using parameters from this work (see Table 4).

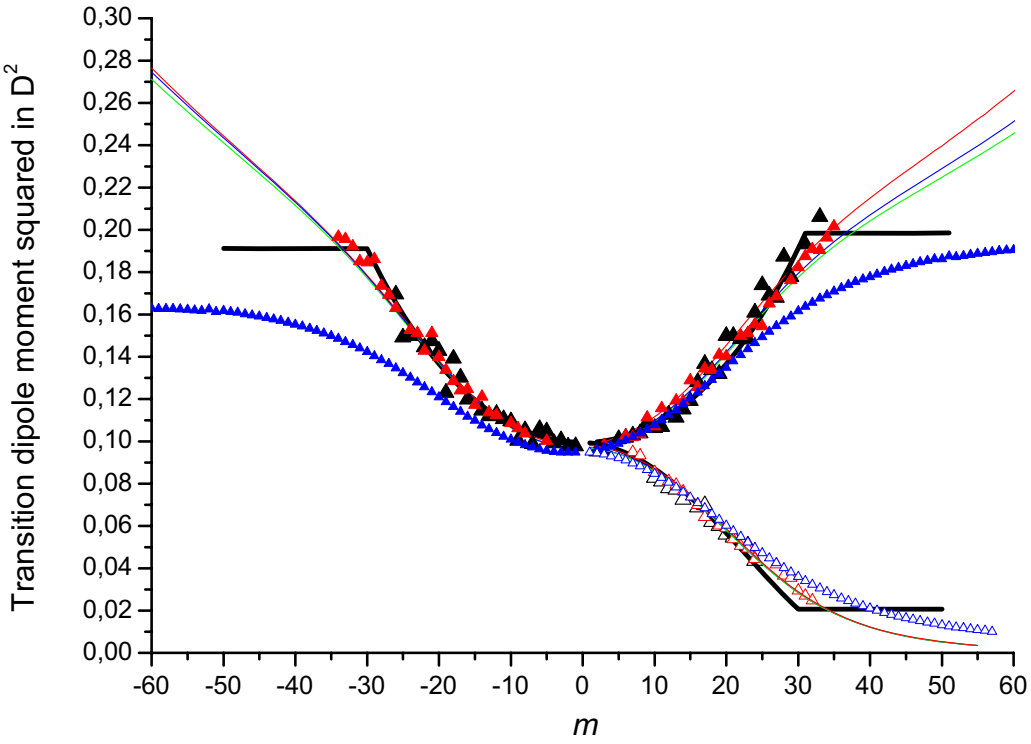

Transition dipole moment squared of transitions belonging to the P_{ee}, R_{ee} and Q_{fe}-branches of the **00002 0 0 – 00001 0 1** band ($2\nu_5^0 - \nu_5^1$) plotted versus m. Black line is from HITRAN [11]. Black and red triangles are measurements from Ref. [13] and the present work respectively (open for Q-branch and solid for P- and R-branches). Calculations obtained using parameters of effective dipole moment are in blue line when using parameters from Ref. [4], in green line when using parameters from Ref. [1], and in red line when using parameters from this work (see Table 4). Plotted in blue symbols (open triangles for Q branch and solid triangles for P and R branches) are transition dipole moment squared from EXOMOL [26].

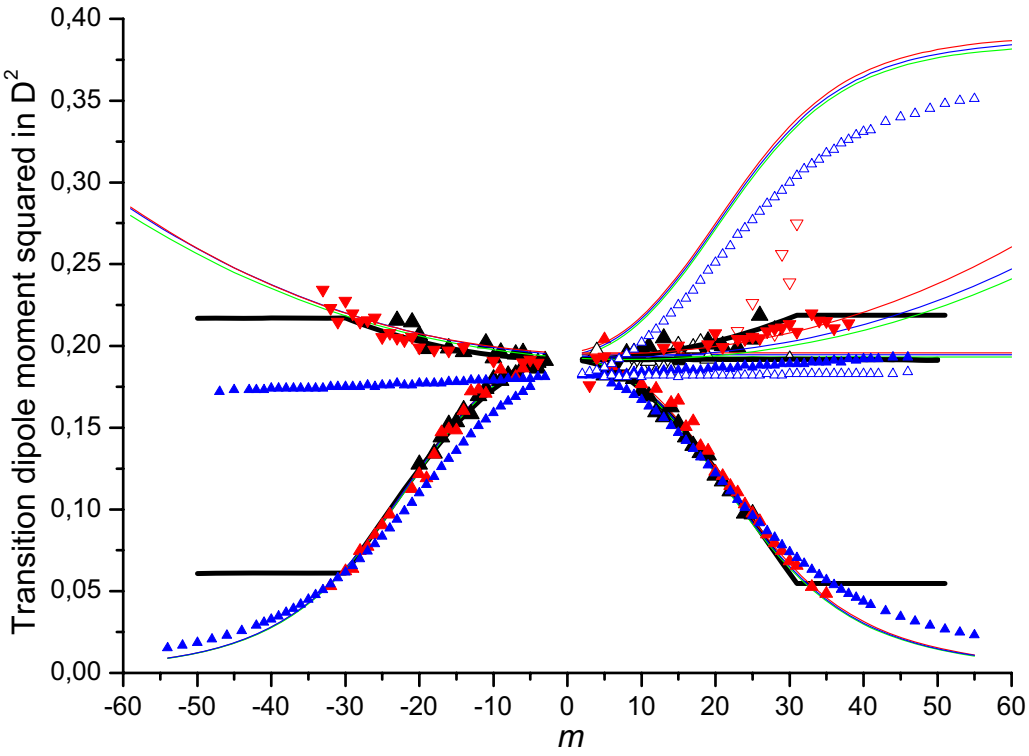

Transition dipole moment squared of transitions belonging to the P_{ee}, R_{ee} ,P_{ff}, R_{ff}, Q_{ef} and Q_{fe}-branches of the **00002 0 2 – 00001 0 1** band plotted versus m (noted $2\nu_5^2 - \nu_5^1$ in Ref. [13] as well as in HITRAN and GEISA databases). Black line is from HITRAN [11]. Black and red triangles are measurements from Ref. [13] and the present work respectively (open for Q-branch and solid for P-and R-branches). Upside triangles are for P_{ee}, R_{ee} and Q_{fe}-branches whereas downside triangles are for P_{ff}, R_{ff} and Q_{ef}-branches. Calculations obtained using parameters of effective dipole moment are in blue line when using parameters from Ref. [4], in green line when using parameters from Ref. [1], and in red line when using parameters from this work (see Table 4). Plotted in blue symbols (open triangles for Q branch and solid triangles for P and R branches) are transition dipole moment squared from EXOMOL [26].

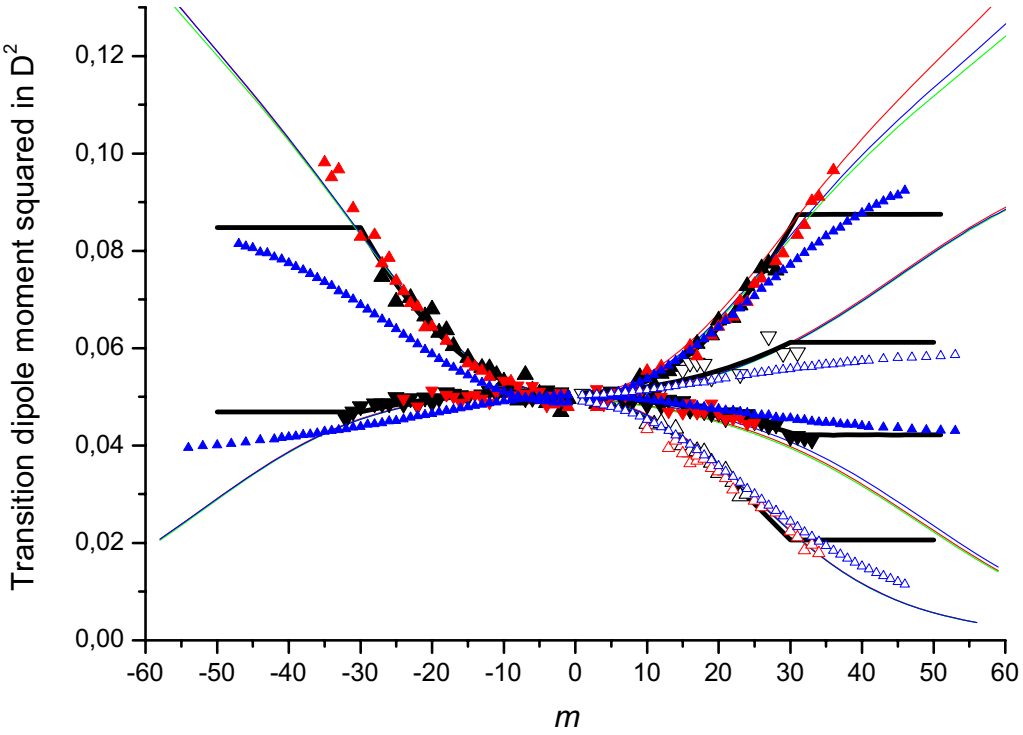

Transition dipole moment squared of transitions belonging to the P_{ee}, R_{ee} ,P_{ff}, R_{ff}, Q_{ef} and Q_{fe}-branches of the **00011 1-1 – 00010 1 0** band plotted versus m (noted $(\nu_4+\nu_5)^0_+ - \nu_4^1$) and $(\nu_4+\nu_5)^0_- - \nu_4^1$ in Ref. [13] as well as in HITRAN and GEISA databases). Black line is from HITRAN [11]. Black and red triangles are measurements from Ref. [Jac2001] and the present work respectively (open for Q-branch and solid for P- and R-branches). Upside triangles are for P_{ee}, R_{ee} and Q_{fe}-branches whereas downside triangles are for P_{ff}, R_{ff} and Q_{ef}-branches. Calculations obtained using parameters of effective dipole moment are in blue line when using parameters from Ref. [4], in green line when using parameters from Ref. [1], and in red line when using parameters from this work (see Table 4). Plotted in blue symbols (open triangles for Q branch and solid triangles for P and R branches) are transition dipole moment squared from EXOMOL [26].

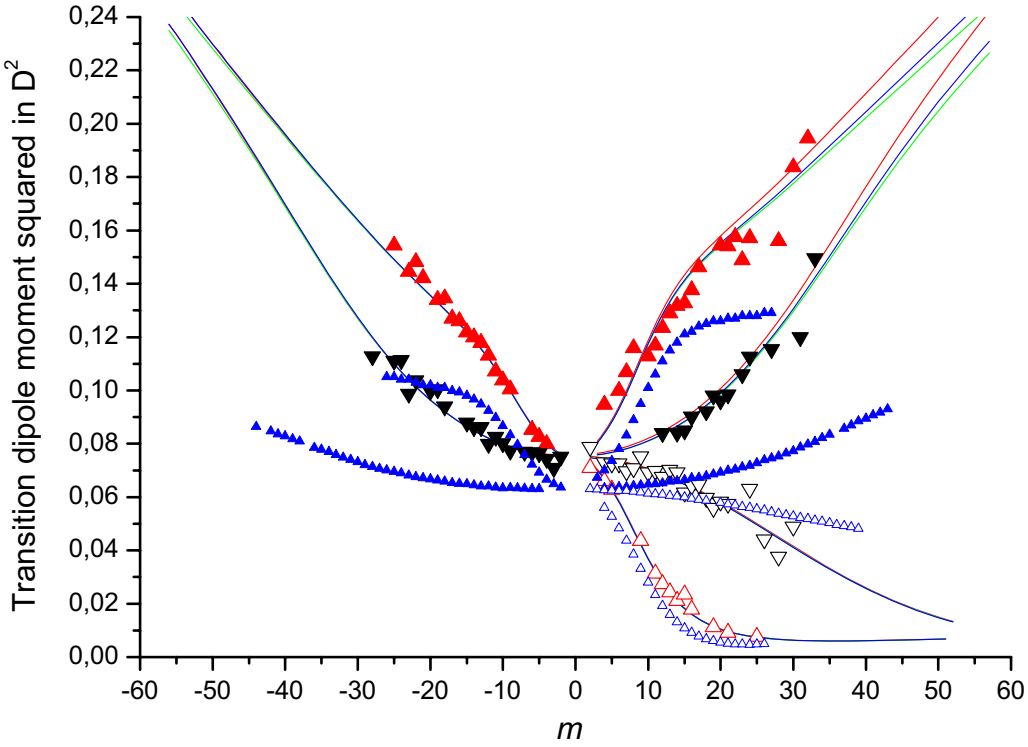

Transition dipole moment squared of transitions belonging to the P_{ee}, R_{ee} ,P_{ff}, R_{ff}, Q_{ef} and Q_{fe}-branches of the 00021 2-1 – 00020 2 0 band plotted versus m. Triangles are measurements from the present work (open for Q-branch and solid for P-and R-branches). Red triangles are for P_{ee}, R_{ee} and Q_{fe}-branches whereas black triangles are for P_{ff}, R_{ff} and Q_{ef}-branches. Calculations obtained using parameters of effective dipole moment are in blue line when using parameters from Ref. [4], in green line when using parameters from Ref. [1], and in red line when using parameters from this work (see Table 4). Plotted in blue symbols (open triangles for Q branch and solid triangles for P and R branches) are transition dipole moment squared from EXOMOL [26].

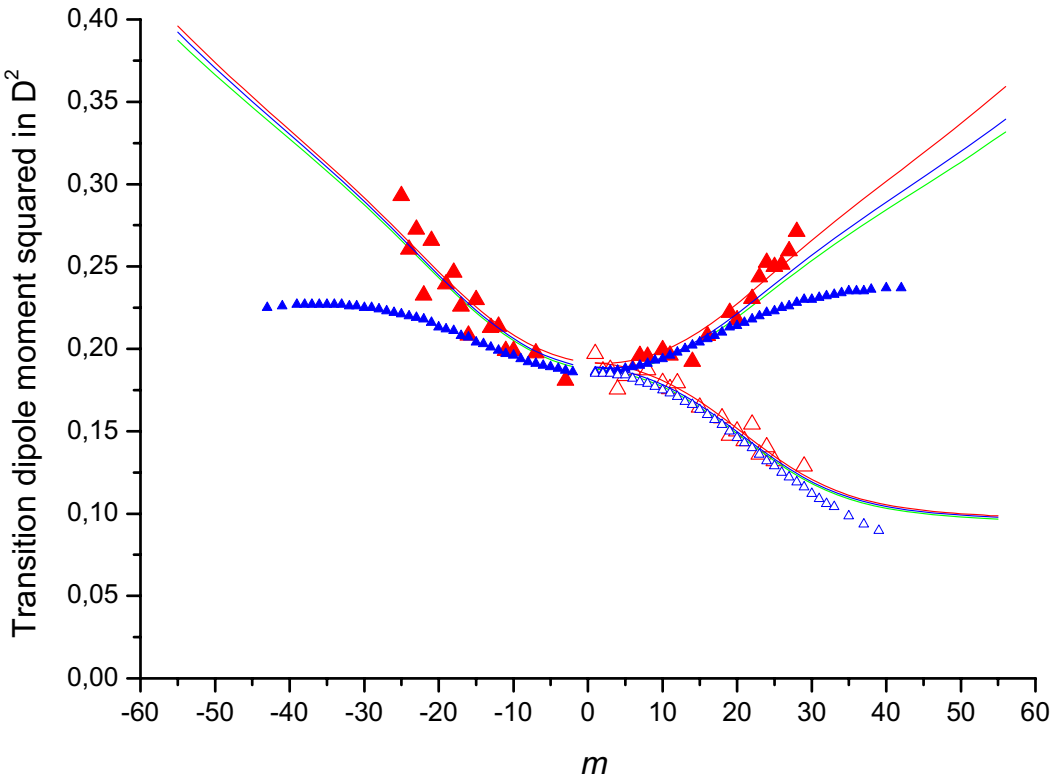

Transition dipole moment squared of transitions belonging to the P_{ee}, R_{ee} and Q_{fe}-branches of the 00003 0 1 – 00002 0 0 band plotted versus m. Triangles are measurements from the present work (open for Q-branch and solid for P-and R-branches). Calculations obtained using parameters of effective dipole moment are in blue line when using parameters from Ref. [4], in green line when using parameters from Ref. [1], and in red line when using parameters from this work (see Table 4). Plotted in blue symbols (open triangles for Q branch and solid triangles for P and R branches) are transition dipole moment squared from EXOMOL [26].

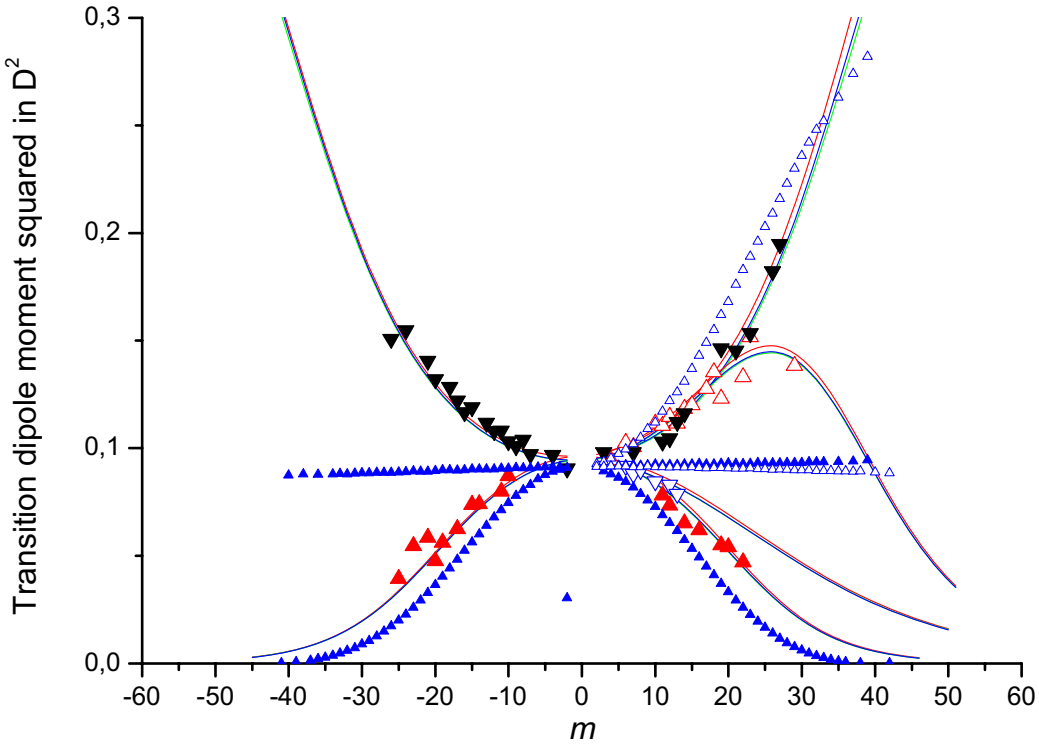

Transition dipole moment squared of transitions belonging to the P_{ee}, R_{ee} ,P_{ff}, R_{ff}, Q_{ef} and Q_{fe}-branches of the **00003 0 1 – 00002 0 2** band plotted versus m. Triangles are measurements from the present work (open for Q-branch and solid for P-and R-branches). Red triangles are for P_{ee}, R_{ee} and Q_{fe}-branches whereas black triangles are for P_{ff}, R_{ff} and Q_{ef}-branches. Calculations obtained using parameters of effective dipole moment are in blue line when using parameters from Ref. [4], in green line when using parameters from Ref. [1], and in red line when using parameters from this work (see Table 4). Plotted in blue symbols (open triangles for Q branch and solid triangles for P and R branches) are transition dipole moment squared from EXOMOL [26].

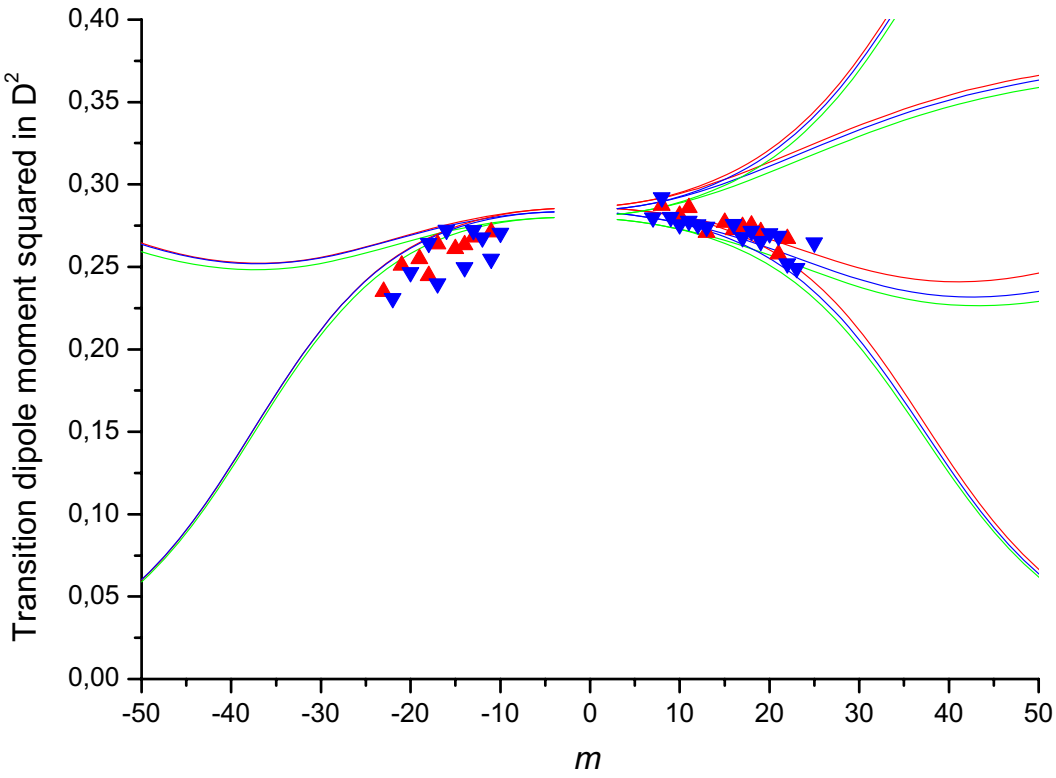

Transition dipole moment squared of transitions belonging to the P_{ee}, R_{ee} ,P_{ff}, R_{ff}, Q_{ef} and Q_{fe}-branches of the **00003 0 3 – 00002 0 2** band plotted versus m. Triangles are measurements from the present work (open for Q-branch and solid for P-and R-branches). Red triangles are for P_{ee} and R_{ee}-branches whereas blue triangles are for P_{ff} and R_{ff}-branches. Calculations obtained using parameters of effective dipole moment are in blue line when using parameters from Ref. [4], in green line when using parameters from Ref. [1], and in red line when using parameters from this work (see Table 4). Not Found in EXOMOL.

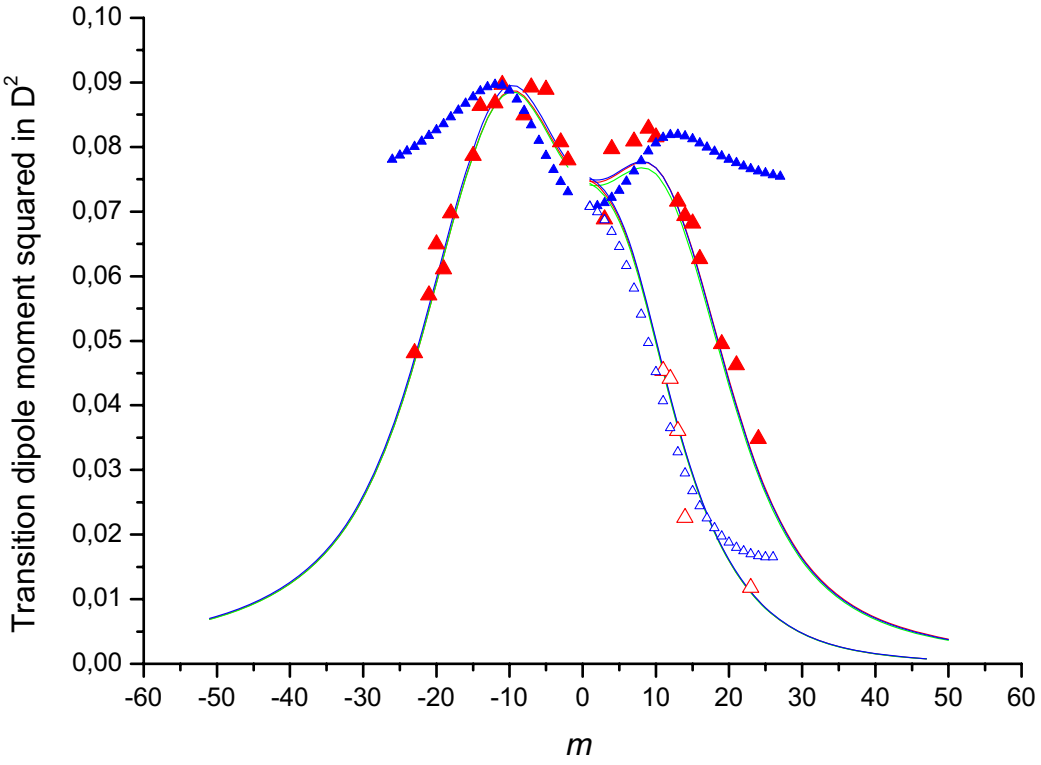

Transition dipole moment squared of transitions belonging to the P_{ee}, R_{ee} and Q_{fe}-branches of the **00021 0 1 – 00020 0 0** band plotted versus m. Red triangles are measurements from this work for the P_{ee}, R_{ee} and Q_{fe}-branches (open triangles for Q-branch and solid ones for P-and R-branches). Calculations obtained using parameters of effective dipole moment are in blue line when using parameters from Ref. [4], in green line when using parameters from Ref. [1], and in red line when using parameters from this work (see Table 4). Plotted in blue symbols (open triangles for Q branch and solid triangles for P and R branches) are transition dipole moment squared from EXOMOL [26].

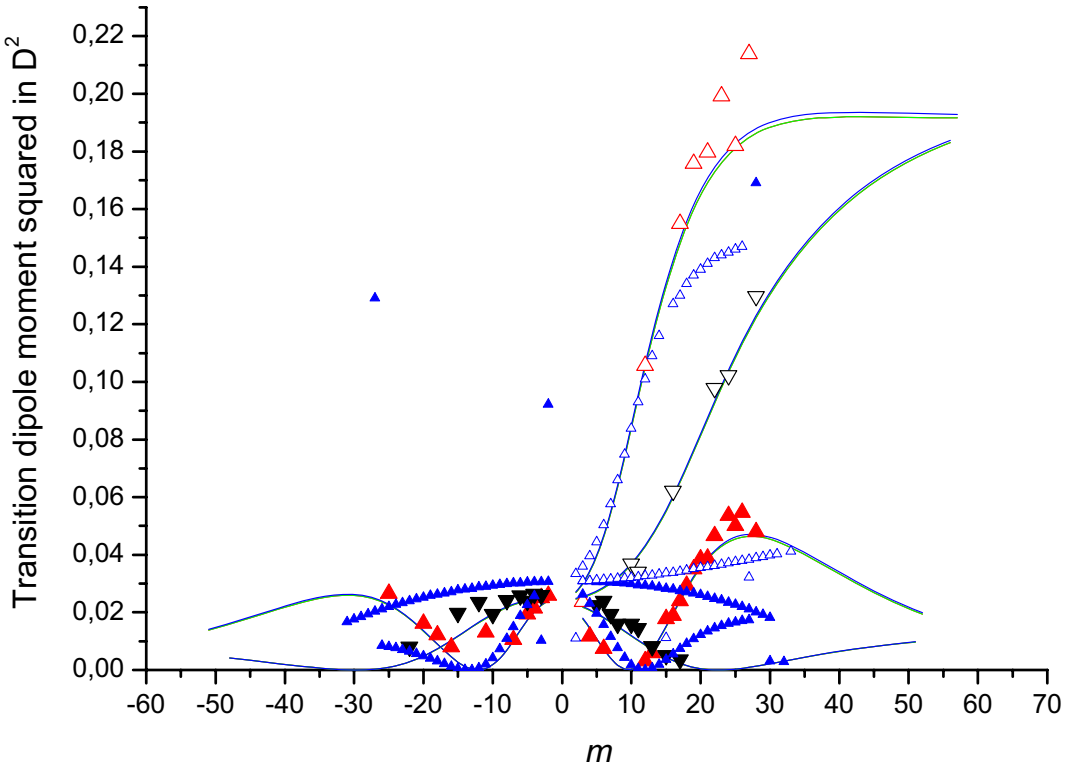

Transition dipole moment squared of transitions belonging to the P_{ee}, R_{ee} ,P_{ff}, R_{ff}, Q_{ef} and Q_{fe}-branches of the **00021 0 1 – 00020 2 0** band plotted versus m. Triangles are measurements from the present work (open for Q-branch and solid for P-and R-branches). Red triangles are for P_{ee}, R_{ee} and Q_{fe}-branches whereas black triangles are for P_{ff}, R_{ff} and Q_{ef}-branches. Calculations obtained using parameters of effective dipole moment are in blue line when using parameters from Ref. [4], in green line when using parameters from Ref. [1], and in red line when using parameters from this work (see Table 4). Plotted in blue symbols (open triangles for Q branch and solid triangles for P and R branches) are transition dipole moment squared from EXOMOL [26].

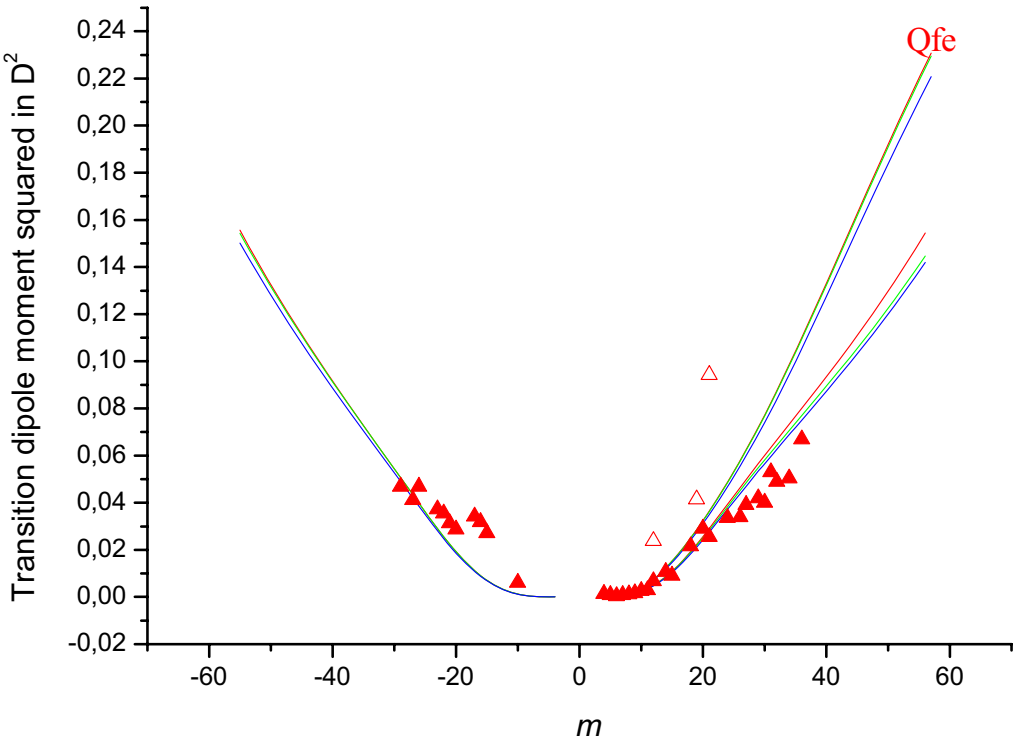

Transition dipole moment squared of transitions belonging to the P_{ee}, R_{ee} and Q_{fe}-branches of the **00021 2 1 – 00020 0 0** band plotted versus m. Red triangles are measurements from this work for the P_{ee}, R_{ee} and Q_{fe}-branches (open triangles for Q-branch and solid ones for P-and R-branches). Calculations obtained using parameters of effective dipole moment are in blue line when using parameters from Ref. [4], in green line when using parameters from Ref. [1], and in red line when using parameters from this work (see Table 4). Not Found in EXOMOL.

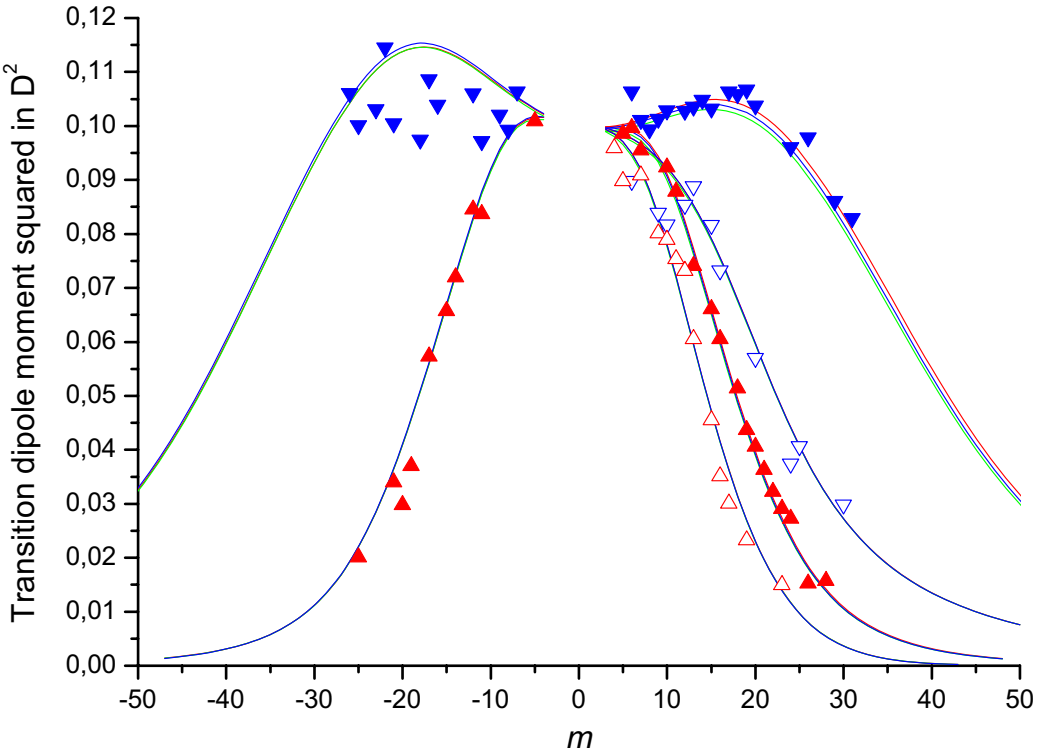

Transition dipole moment squared of transitions belonging to the P_{ee}, R_{ee} ,P_{ff}, R_{ff}, Q_{ef} and Q_{fe}-branches of the **00021 2 1 – 00020 2 0** band plotted versus m. Triangles are measurements from the present work (open for Q-branch and solid for P-and R-branches). Red triangles are for P_{ee}, R_{ee} and Q_{fe}-branches whereas blue triangles are for P_{ff}, R_{ff} and Q_{ef}-branches. Calculations obtained using parameters of effective dipole moment are in blue line when using parameters from Ref. [4], in green line when using parameters from Ref. [1], and in red line when using parameters from this work (see Table 4). Not Found in EXOMOL.

I checked by plotting synthetic spectra around the R20f quite visible in our exp spectra at 783.8717 cm^{-1}, the most intense below (in blue EXOMOL, green HITRAN 2016, red ASD).

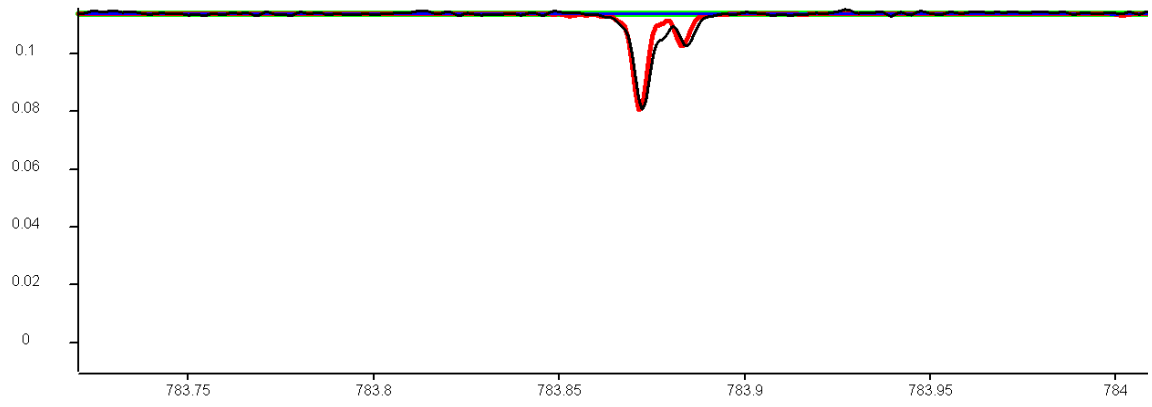

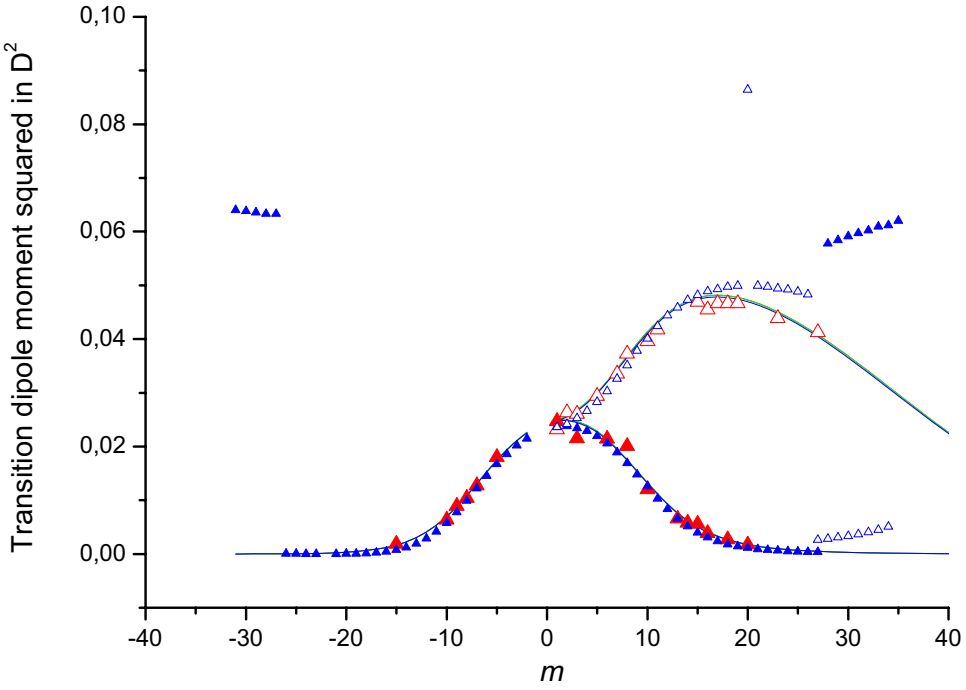

Transition dipole moment squared of transitions belonging to the P_{ee}, R_{ee} and Q_{fe}-branches of the **00021 2-1 – 00020 0 0** band plotted versus m. Red triangles are measurements from this work for the P_{ee}, R_{ee} and Q_{fe}-branches (open triangles for Q-branch and solid ones for P-and R-branches). Calculations obtained using parameters of effective dipole moment are in blue line when using parameters from Ref. [4], in green line when using parameters from Ref. [1], and in red line when using parameters from this work (see Table 4). Plotted in blue symbols (open triangles for Q branch and solid triangles for P and R branches) are transition dipole moment squared from EXOMOL [26].

Line P27e at 641.4486 has strange R2 value around 0.06 D2. And indeed the EXOMOL synthetic spectrum (in blue) presents a line that is not observed.

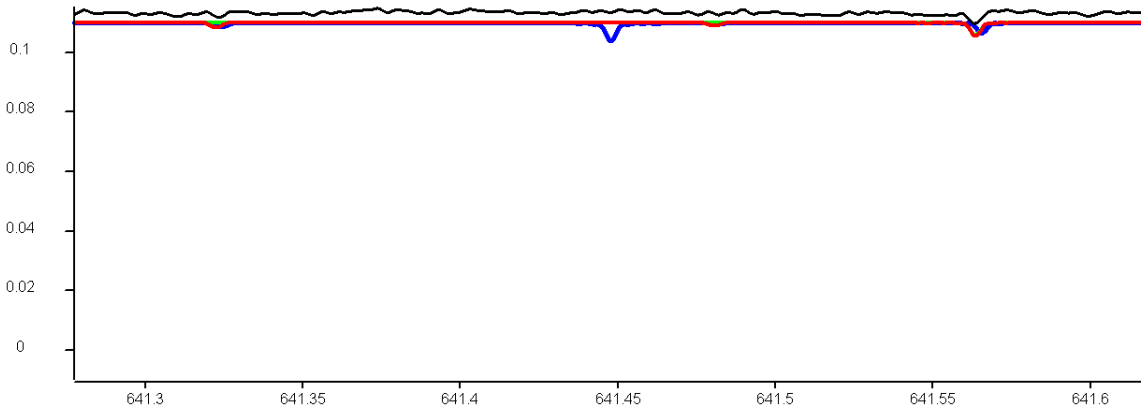

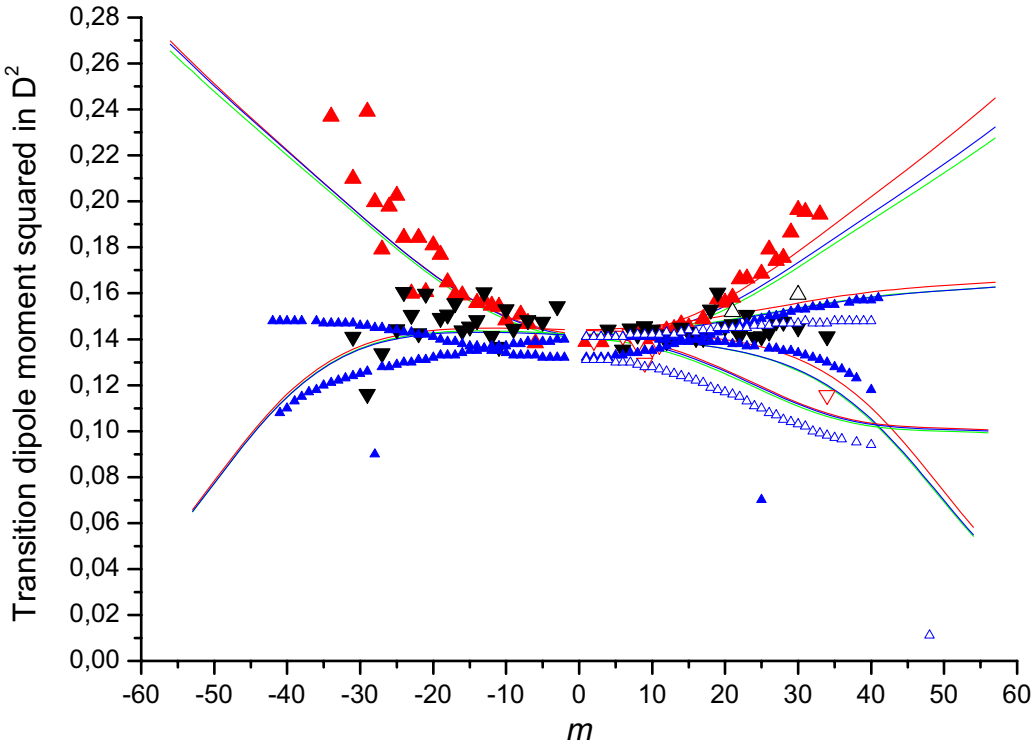

Transition dipole moment squared of transitions belonging to the P_{ee}, R_{ee} ,P_{ff}, R_{ff}, Q_{ef} and Q_{fe}-branches of the **00012 1 0 – 00011 1-1** band plotted versus m. Triangles are measurements from the present work (open for Q-branch and solid for P-and R-branches). Red triangles are for P_{ee}, R_{ee} and Q_{fe}-branches whereas black triangles are for P_{ff}, R_{ff} and Q_{ef}-branches. Calculations obtained using parameters of effective dipole moment are in blue line when using parameters from Ref. [4], in green line when using parameters from Ref. [1], and in red line when using parameters from this work (see Table 4). Plotted in blue symbols (open triangles for Q branch and solid triangles for P and R branches) are transition dipole moment squared from EXOMOL [26].

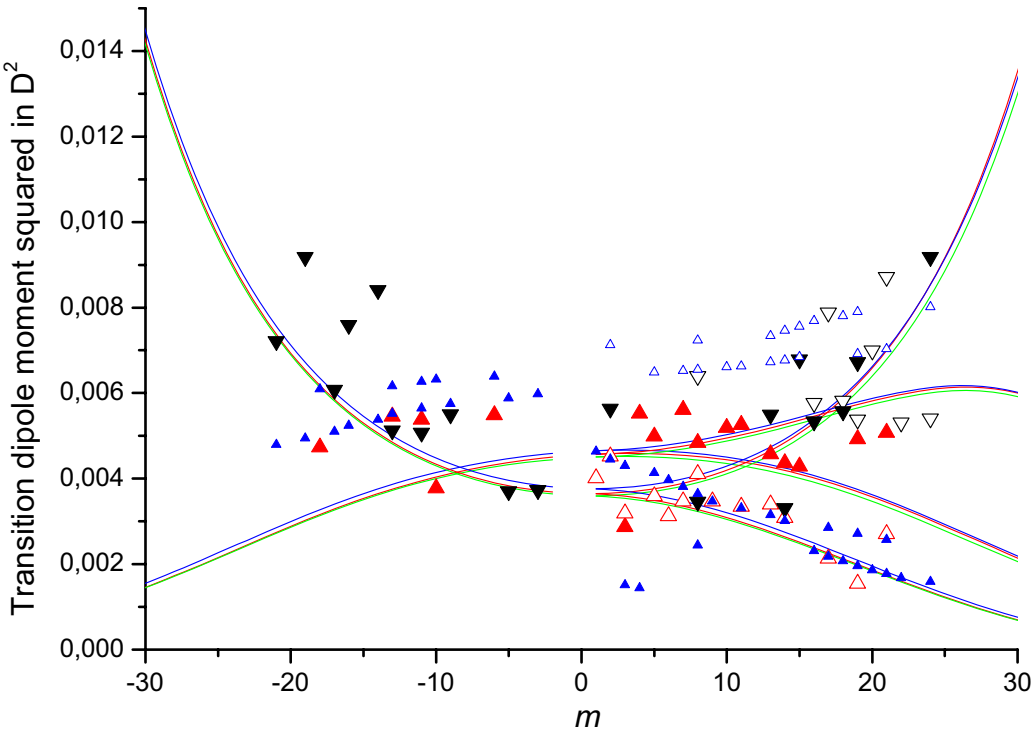

Transition dipole moment squared of transitions belonging to the P_{ee}, R_{ee} ,P_{ff}, R_{ff}, Q_{ef} and Q_{fe}-branches of the **00012-1 2 – 00011 1-1** band plotted versus m. Triangles are measurements from the present work (open for Q-branch and solid for P-and R-branches). Red triangles are for P_{ee}, R_{ee} and Q_{fe}-branches whereas black triangles are for P_{ff}, R_{ff} and Q_{ef}-branches. Calculations obtained using parameters of effective dipole moment are in blue line when using parameters from Ref. [4], in green line when using parameters from Ref. [1], and in red line when using parameters from this work (see Table 4). Plotted in blue symbols (open triangles for Q branch and solid triangles for P and R branches) are transition dipole moment squared from EXOMOL [26].

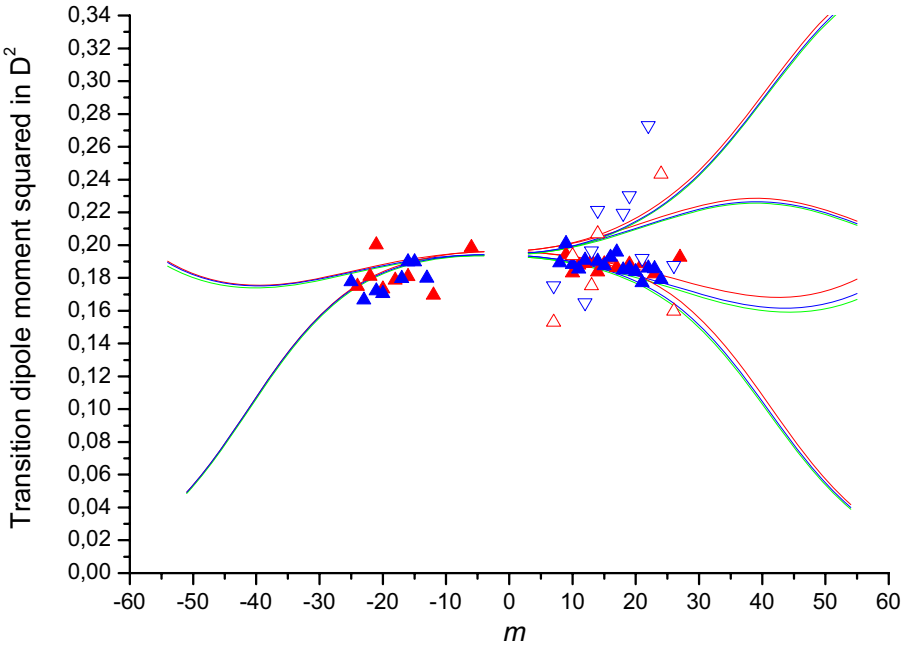

Transition dipole moment squared of transitions belonging to the P_{ee}, R_{ee} ,P_{ff}, R_{ff}, Q_{ef} and Q_{fe}-branches of the **00012 1 2 – 00011 1 1** band plotted versus *m*. Triangles are measurements from the present work (open for *Q*-branch and solid for *P*-and *R*-branches). Red triangles are for P_{ee}, R_{ee} and Q_{fe}-branches whereas blue triangles are for P_{ff}, R_{ff} and Q_{ef}-branches. Calculations obtained using parameters of effective dipole moment are in blue line when using parameters from Ref. [4], in green line when using parameters from Ref. [1], and in red line when using parameters from this work (see Table 4). Not Found in EXOMOL.

Below at 750.378 cm-1, the Rff7 of this band observed in exp spectrum (black line) is reproduced by our line list (ASD in red), but not by HITRAN or EXOMOL. Around 750.56, two lines are also missing in EXOMOL, the Ree8 and Rff8 of 000 0 3 0 3 _ u 000 0 2 0 2 g band also missing in EXOMOL. The transitions with stars correspond to $^{12}C^{13}H_2$ transitions.

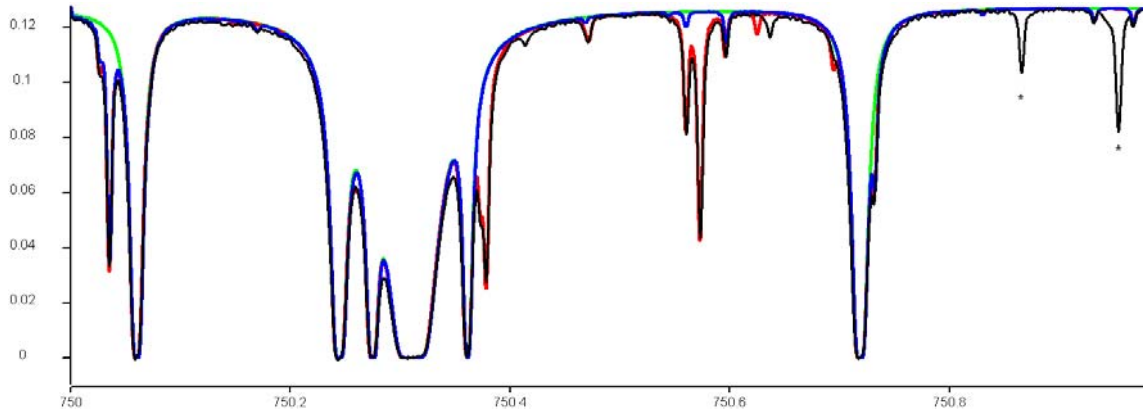

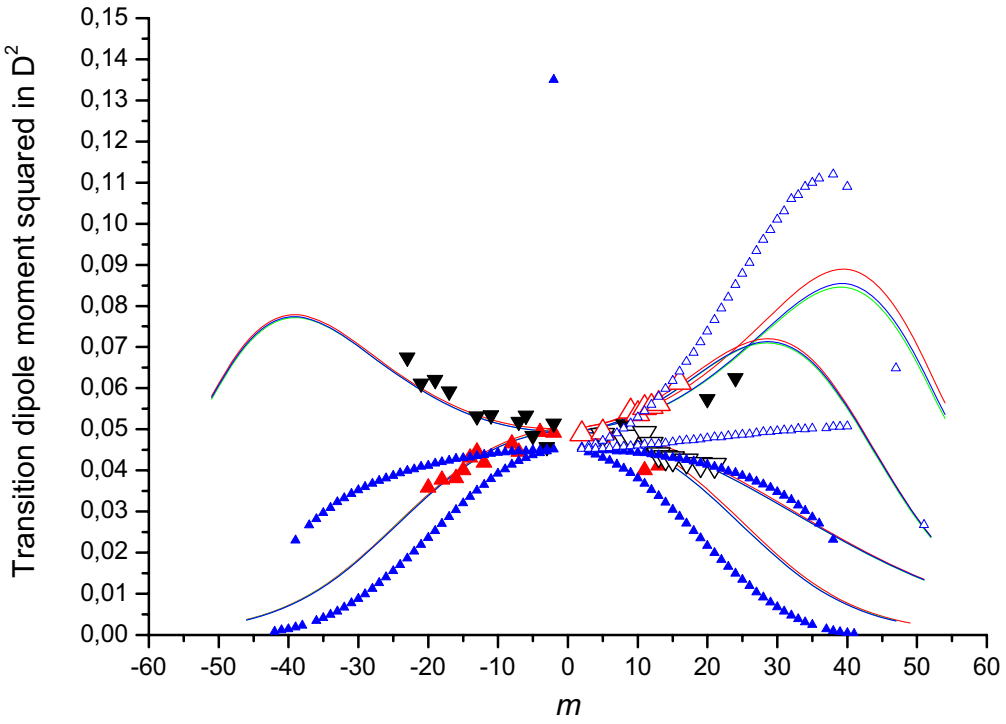

Transition dipole moment squared of transitions belonging to the P_{ee}, R_{ee} ,P_{ff}, R_{ff}, Q_{ef} and Q_{fe}-branches of the **00012 1 0 – 00011 1 1** band plotted versus m. Triangles are measurements from the present work (open for Q-branch and solid for P-and R-branches). Red triangles are for P_{ee}, R_{ee} and Q_{fe}-branches whereas blue triangles are for P_{ff}, R_{ff} and Q_{ef}-branches. Calculations obtained using parameters of effective dipole moment are in blue line when using parameters from Ref. [4], in green line when using parameters from Ref. [1], and in red line when using parameters from this work (see Table 4). Plotted in blue symbols (open triangles for Q branch and solid triangles for P and R branches) are transition dipole moment squared from EXOMOL [26].

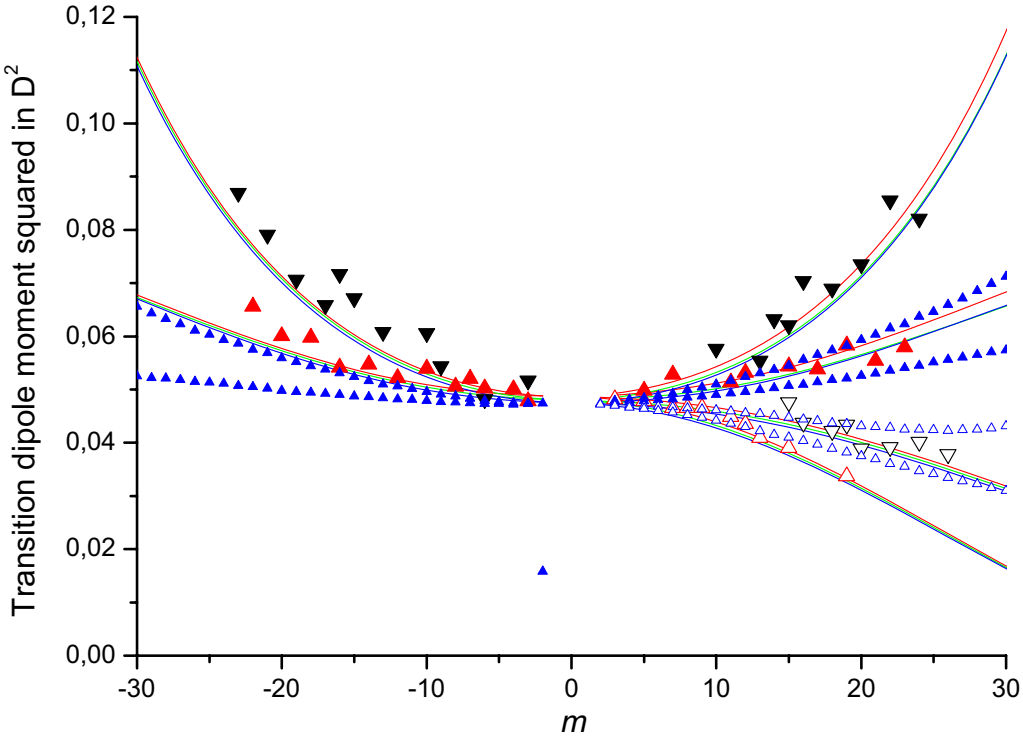

Transition dipole moment squared of transitions belonging to the P_{ee}, R_{ee} ,P_{ff}, R_{ff}, Q_{ef} and Q_{fe}-branches of the **00012-1 2 – 00011 1 1** band plotted versus m. Triangles are measurements from the present work (open for Q-branch and solid for P-and R-branches). Red triangles are for P_{ee}, R_{ee} and Q_{fe}-branches whereas black triangles are for P_{ff}, R_{ff} and Q_{ef}-branches. Calculations obtained using parameters of effective dipole moment are in blue line when using parameters from Ref. [4], in green line when using parameters from Ref. [1], and in red line when using parameters from this work (see Table 4). Plotted in blue symbols (open triangles for Q branch and solid triangles for P and R branches) are transition dipole moment squared from EXOMOL [26].